OPTIMISATION OF ORMOSIL THIN FILMS FOR SENSOR APPLICATIONS

By

PENNY LAVIN, B.Sc.

Submitted for the Degree of

MASTER OF SCIENCE

Presented to

DUBLIN CITY UNIVERSITY

Research Supervisor

DR. COLETTE McDONAGH,
School of Physical Sciences,
Dublin City University.

OCTOBER 1997

Abstract

Sol-Gel derived thin films are becoming increasingly important for optical sensor applications. Analyte-sensitive dyes are easily entrapped in the porous film while remaining accessible to the analyte, and the nature of the sol-gel process lends flexibility to film fabrication, in particular enabling tailoring of film properties for specific sensor applications.

Recent work has indicated the ormosil films, fabricated from organically modified precursors, produce better sensor performance for some specific applications, compared to films from conventional sol-gel precursors such as tetraethoxysilane (TEOS) or tetramethoxysilane (TMOS). This project aims to compare film properties and sensor behaviour for films fabricated from different organically modified precursors. Microstructural differences, for example porosity changes due to the different precursor backbone structures, are investigated by monitoring sensor response. Sol-Gel fabrication parameters such as sol pH and R-value are varied. Resulting film properties such as thickness, thickness stabilisation time and sensor response are discussed in terms of relative hydrolysis and condensation behaviour for the different precursors. Issues that have been identified as being of crucial importance for optimum sensor response, such as dye leaching, film surface hydrophobicity and humidity response are discussed for both film types. The motivation for this work is film optimisation for optical sensors in particular gas phase and dissolved oxygen sensors.

Dedication

To Mum and Dad,

for the millions of little things (and the many, many big things!).

Acknowledgements

I would like to take this opportunity to thank everyone who helped and encouraged me throughout this project. Most especially thanks to Colette for giving me the chance to do this programme and for all her support throughout. Thanks also to Brian for his helping hand. To all the technicians, Des, Alan, Al, Joe and John for their help with the equipment. Thanks also to Brian Lawless for his help. To Marion and Alison. To all the lads and lassies in the physics department for all the moan and groan sessions especially Terri, Deirdre, Eilish, Catherine, Charles and Sean, thanks! To Anto my nurophen munching partner in the girlie lab and the lads up stairs, Aidan, Colm, Paud and Chris. Thanks to Jeff for the help with the photographs. Thanks also to sol-gel group past for helping me find my feet, Ais, Tom and Vince.

To John, John, Pam and Ellen (the greatest baby in the world!) and also my brother Greg and my sister Sarah, for putting up with me! To Joe and Hadas for the transport over the last year or so. To Lena and Katie for support from across the water. Finally to Mum and Dad for all their help and encoragement.

Table of Contents

Chapter 1

Introduction

1.1 Introduction

The sol-gel process is a series of reactions under controlled conditions that allows a solution or *sol* to form a crosslinked matrix or *gel*. This process can give rise to high surface area, porous products, which can be used as support matrices for optical sensors. This project deals with sol-gel derived thin films doped with a ruthenium complex whose fluorescence is quenched in the presence of oxygen. The main aim of the project is to fabricate and characterise sol-gel sensor films in order to tailor processing parameters to optimise gas phase and dissolved oxygen sensor performance. This chapter introduces optical oxygen sensing and the sol-gel process.

1.2 Optical Sensors and Oxygen Monitoring

A sensor is a device that can record a physical parameter or the concentration of a chemical, analyte or biochemical species. Optical sensors achieve this by measuring a change in optical properties as a function of the particular parameter. This can be through the measurement of reflection, scattering, interference, fluorescence, absorption or refraction of light. When such a change occurs, it can be observed by

the modulation of either wavelength, amplitude, phase or polarisation. There has been a lot of research in the area of optical sensors in the last twenty years. Optical sensors can offer many advantages over other sensor types for example, ease of miniaturisation, lack of susceptibility to electrical interference, compatibility with optoelectronic devices such as light emitting diodes and photodiodes

Fluorescence based sensors have high sensitivity and selectivity. It is possible to make these sensors small, light weight and portable[1]. Oxygen is one of the most widely measured parameters particularly in environmental monitoring. The most common method of measuring oxygen concentration is by the Clarke electrode[2]. This has the disadvantage that it consumes oxygen and has a slow response time. There is a market for alternative oxygen measuring technology which has a faster response time and does not consume oxygen and the sol-gel based oxygen sensor research programme in this laboratory aims to serve that market. In this project a fluorescence sol-gel based oxygen sensor based on the collisional quenching by molecular oxygen of a fluorophore entrapped in a sol-gel matrix is used as a model system to investigate the effect of different sol-gel precursors on sensor performance.

1.3 Sol-Gel Thin Films

The sol-gel process for making glasses and ceramics at low temperature provides a wide basis for research and development. Using this process it is possible to make coatings, fibres and monoliths[3]. This project studies sol-gel coatings in the form of thin films.

The actual sol-gel process is discussed in more detail in chapter 2 and is ideal for preparing thin films by processing the fluid sol either by dipping, spin coating or

spraying. These methods of producing thin films use less equipment and are less expensive than conventional methods such as evaporation or sputtering. The coatings produced are chemically inert and thermally stable. They are also intrinsically bound to the substrate. However the most important advantage of sol-gel processing over conventional methods is that it is possible to control the properties, such as the microstructure, of the deposited film[4]. This makes them attractive for use as support matrices for sensors.

By using the sol-gel process it is possible to incorporate sensing materials into the matrix and by doing this the thin films prepared can be used for sensing. In 1991 McCraith *et al* [5] used this principle to develop a fibre optic pH sensor. This was achieved by immobilising a pH indicator in a silica gel matrix and then coating onto optical fibres. Since then optical fibre sensing using sol-gel films has been reported by many groups for the sensing of a wide range of analytes, including sensors for metal ions[6] and biomolecules[7]. This laboratory has reported the use of sol-gel thin films on fibres, planar substrates and planar waveguides for sensing gasphase oxygen, dissolved oxygen, ammonia and pH[5,8,9,10]. In this project an oxygen sensitive ruthenium complex, oxygen sensitive $[Ru(II)(Ph_2Phen)_3]^{2+}$,is incorporated into the sol-gel matrix and then coated onto planar substrates. Since the sol-gel network is porous it allows small molecules (such as oxygen) to access the immobilised ruthenium. In the absence of oxygen this complex fluoresces and the fluorescence is quenched in the presence of oxygen.

1.4 Motivation

This project was motivated by the need to characterise sol-gel derived thin films for optical sensor applications in order to determine the optimum film fabrication parameters. A lot of work has been carried out on the characterisation of films fabricated using tetraethoxysilane (TEOS)[11]. In this project a range of precursors have been used including TEOS as discussed in the next chapter.

1.4.1 Objectives

Factors governing sensor response are detailed in the following chapters. Properties such as film thickness and stabilisation time, hydrophobicity and sensor performance are all important when choosing a sensor film fabricated from a particular precursor. This project aims to characterise films fabricated using a range precursors in order to find an optimum sensor film for gas phase and dissolved oxygen sensing.

1.5 References

[1] A.K. McEvoy; **Development of an Optical Sol-Gel-Based Dissolved Oxygen Sensor**, PhD. Thesis, 1996, Dublin City University (unpublished).

[2] L.C. Clark, Jr.; **Monitor and Control of Blood and Tissue Oxygen Tensions**, *Trans. Amer. Artif. Intern. Organs*, 1956, Vol.2, pp.41.

[3] L.C .Klein; **Sol-Gel Glass Technology, A Review,** *Glass ind* 1981 vol. 14 pp 17

[4] C.J. Brinker, G.W. Scherer; **Sol-Gel Science: The Physics and Chemistry of Sol-Gel Processing**, Academic Press, San Diego, 1990, pp. 787.

[5] B.D. MacCraith, V. Ruddy, C. Potter, B O'Kelly, J.F. McGilp; **Optical Waveguide Sensor using Evanescent Wave Excitation of Fluorescent Dye in Sol-Gel Glass,** *Electron. Lett.,* Vol. 27 No.14, 1991, pp. 1247-1248.

[6] J.Y. Ding, M.R. Shahriari, G.H. Siegel, Jr.; **Fibre Optic pH Sensors Prepared by Sol-gel Immobilisation Technique**, *Electron. Lett.*, Vol.17 No. 27, pp. 1560-1561.

[7] D.J. Blyth, J.W. Aylott, D.J. Richardson, D.A. Russell; **Sol-Gel Encapsulation of Metalloproteins for the Development of Optical Biosensors for Nitrogen Monoxide and Carbon Monoxide,** *The Analyst*, 1995, Vol. 120, pp. 2725.

[8] B.D .MacCraith, G. O'Keeffe, A.K. McEvoy, C.M. McDonagh: **Development of a LED-based Fibre-optic oxygen sensor using sol-gel-derived coatings,** *Proc. SPIE*, 1994, Vol. 2293, pp.110.

[9] A.K. McEvoy, C.M. McDonagh, B.D. MacCraith **Dissolved Oxygen Sensor Based on Fluorescence Quenching of Oxygen-Sensitive Ruthenium Complexes Immobilised in Sol-Gel-Derived Porous Silica Coatings,** *The Analyst*, 1996, 121, 785-788.

[10] A. Doyle, B.D. MacCraith; **Fabrication of sol-gel based planar waveguide/ grating coupler platforms for use as optical chemical sensors**, *Proc. SPIE*, 1997, Vol. 3105, pp.61-70.

[11]C.M. McDonagh, F. Sheridan, T Butler, B.D. MacCraith; **Characterisation of Sol-Gel-Derived Silica Films**, *J. Non-Cryst. Solids,* 1996, Vol. 194 pp. 72-77.

Chapter 2

The Sol-Gel Process and Thin Film Fabrication

2.1 Introduction

This chapter explains the steps involved in the sol-gel process from the chemistry of the reactions to the formation of thin films. It also discusses the different parameters that are involved in the fabrication of sol-gel derived thin films.

2.2 The Sol-Gel Process

The sol-gel process is a method for preparing speciality metal oxide glasses and ceramics at low temperatures. This is achieved by the hydrolysis and condensation of metal precursors, whereby a one phase solution undergoes a transition to become a rigid porous network, a two phase system of solid metal oxide and solvent filled pores. The most widely used precursors in sol-gel research are metal alkoxides for example tetraethoxysilane (TEOS). TEOS is a metalloid oxide in which an organic ligand i.e. an alkoxide is attached to central silicon atom. This class is popular because they react readily with water via hydrolysis.

2.2.1 Hydrolysis and Condensation

Most techniques for the sol-gel process use water, low molecular mass alkoxysilanes (e.g. TEOS or TMOS - *tetramethloxysilane*) as precursors. A solvent is used because alkoxysilanes are not miscible with water although it is not strictly necessary[1] since hydrolysis generates sufficient alcohol eventually. Ethanol is most commonly used. A catalyst is also used which can be either acid or base depending on the reaction route preferred For this project HCl is used as an acid catalyst.

The sol-gel route consists of two basic reactions:

1. The hydrolysis of the metal alkoxide by nucleophilic attack by the oxygen in the water on the silicon atom[2]. The reverse reaction of this is esterification of silanol from alcohol

$$: Si - OR + H_2O \Leftrightarrow : Si - OH + ROH \qquad (2.1)$$

2. A 3D network is built up by two types of nucleophilic condensation reactions which produce siloxane bonds $: Si - O - Si :$

This is achieved by:

a) Water Condensation

$$: Si - OH + HO - Si : \Leftrightarrow : Si - O - Si : + H_2O \qquad (2.2)$$

b) Alcohol Condensation

$$: Si - OR + HO - Si : \Leftrightarrow : Si - O - Si : + ROH \qquad (2.3)$$

2.3 Processing Parameters

2.3.1 pH of Sol

One of the most important parameters in the sol-gel process is the pH of the starting solution. The isoelectric point is where surface charge is zero, for silica this occurs at approximately pH=2. This pH forms the boundary between acid catalysis pH<2 and base catalysis, pH>2 of the process.

Acid catalysis is associated with fast hydrolysis and relatively long gel times whereas base catalysis gives slow hydrolysis but the gel times are faster due to faster condensation rates. Under basic conditions more dense colloidal particles are formed with large interstices between them. Acid conditions give a gel formed from a fine network structure of linear chains[3]. Figure 2.1 shows the pH dependence of the gel time of sols catalysed by different acids [gel time $\propto$ 1/ Average condensation rate]. According to the graph the condensation rate is minimised at ~ pH = 1.5 - 2.0.

Reaction schemes

Acid Catalysis

There has been a lot of research on the proposed mechanism for acid catalysed sol-gel processing[4], although Pohl and Osterholz reaction is the most favoured (shown in figure 2.2). They propose a mechanism in which an alkoxide group is protonated in a rapid first step which causes electron density to be withdrawn from silicon. This makes the silicon more electrophilic and hence more susceptible to attack by water.

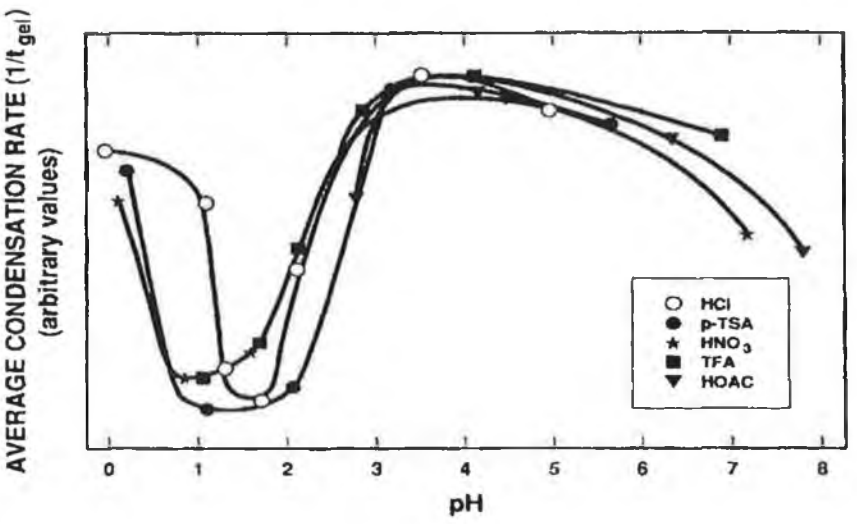

Figure 2.1 pH dependence of gel time for TEOS hydrolysed with solutions of different acids[2].

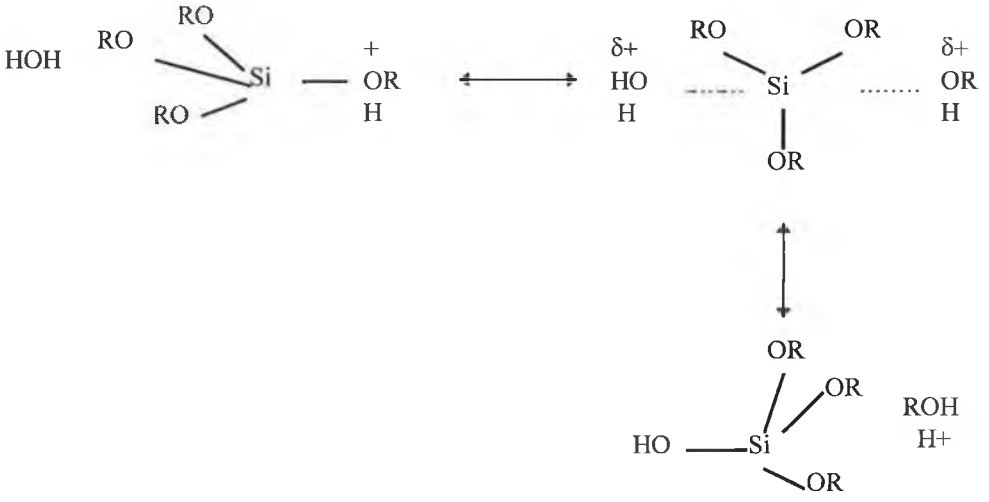

Figure 2.2 Acid Catalysed Mechanism

According to Pohl and Osterholz the transition state has a significant S_N2 type character, the water attacks from the rear and aquires a partial positive charge. This

reduces the positive charge of the protonated alkoxide and makes alcohol a better leaving group and so alcohol is displaced and the silicon tetrahedron is inverted.

This mechanism is dependent on steric crowding whereby the hydrolysis rate is increased by substituents that reduce steric crowding. Therefore we would expect precursors such as TMOS to have faster hydrolysis rates than TEOS. Although silicon aquires little charge in the transition state, electron- providing substituents for example alkyl groups should also slightly increase the rate of hydrolysis because they help to stabilise the developing positive charge.

Base catalysis

The mechanism for base catalysis was proposed by Iler[5] shown in figure 2.3. In this mechanism water dissociates to produce nucleophilic hydroxyl anions in a rapid first step. The anion attacks the silicon atom in an S_N2 type reaction in which OH^- displaces OR^- with inversion of the silicon tetrahedron

Factors such as steric hindrance and inductive effects will affect the hydrolysis rates.

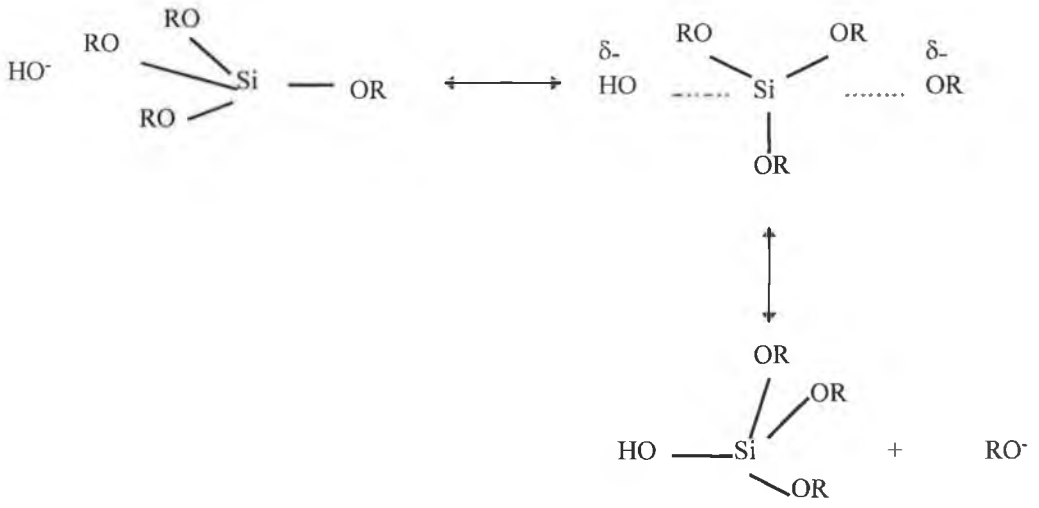

Figure 2.3 Base Catalysed Mechanism

2.3.2 Ratio of water to precursor, R value

The R value of a sol is the molar ratio of water to precursor. The amount of water used in the sol-gel process influences the structure of the final gel because it is used in the hydrolysis reaction and evolved in the condensation reaction. R=2 is the stoichiometric water: precursor ratio and theoretically the R value for complete hydrolysis and condensation. However due to the formation of intermediate species and reverse reactions it is not usually sufficient.

For acid catalysis the R value of a sol will decrease the gel time at a given pH up to the point where it starts to dilute the sol. This only happens at high R values, for example ~ R=9[2]. The R value where dilution becomes a factor is dependent on the experimental conditions involved.

2.3.3 Ageing Time

Since the object of this project is the formation of thin films, after stirring, the sol is used to coat substrates to form a film. In some cases the sol does not coat the substrate straight away and so the sol is left to *age* either at room temperature or at 70°C. The viscous sol is then able to coat the substrate.

2.4 Thin Film Fabrication

Prior to gelation the sol can be deposited onto substrates to form thin films. This can be done by dip coating or spin coating. Spin coating is achieved by depositing a few drops of sol on the surface of the substrate. These substrates are then spun around to produce a film[6]. This method has the advantage that there is little waste, however it

does not work well for large substrates or substrates that are not circular. Since dip coating is suitable for substrates of any shape or size it was more suitable for this experiment.

2.4.1 Dip Coating

Dip coating onto substrates involves the substrate being immersed in a reservoir of sol and then withdrawn vertically at a constant speed. The films made for this project were deposited using a computer controlled dip coating apparatus shown in figure 2.4.

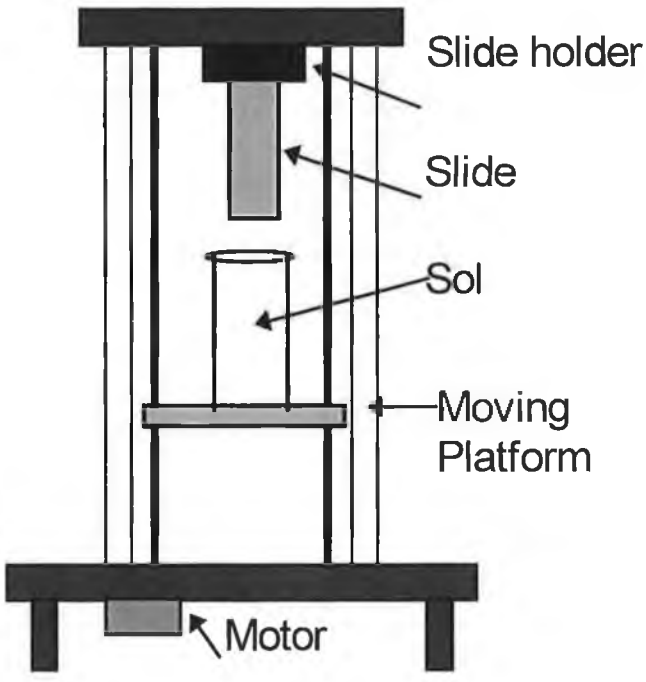

Figure 2.4 Dip-Coating Apparatus

The dip coater raises the platform with the sol reservoir to the substrate which is held above. When the substrate has been immersed, the platform can be lowered depositing the film on the substrate. The film is left to reach equilibrium where there is flow of

sol from the top of the film leaving a small uneven deposit. It has been shown that the withdrawal speed has an effect on the film thickness as discussed in section 5.3.1[7]. For this project all films were dipped at constant withdrawal speed of 1 mm/sec. Coatings were carried out in a draught free environment using a perspex covering as a draught guard. A vibration free environment was achieved by incorporating vibration dampers into the apparatus.

2.4.2 Effect of Substrate

To produce a durable, uniform thin film the substrate should be clean, with no grease or dust particles on the surface that is being coated. It should also be even and preferably polished. Variations in substrate surface will give rise to non-uniformity of film thickness. For this project films are coated onto planar substrates of glass and silicon. Glass substrates are prepared from soda-lime microscope slides cut into quarters and silicon substrates are prepared from silicon wafers. The substrates are cleaned by washing with deionised water then methanol, acetone and finally deionised water again. The substrates are then placed in deionised water at 70°C for 24 hours. This is thought to condition the slides by increasing the number of surface silanol groups and hence improve adhesion of the sol-gel film to the substrate.

2.5 Ormosils

Ormosils are *or*ganically *mo*dified *sil*anes, where one or more of the alkoxide groups are replaced by organic groups for example methyl or ethyl groups. Ormosils possess great potential because organic groups can bring new properties to the inorganic

network including flexibility, hydrophobicity and refractive index modifications[8]. By using modified precursors it is possible to bring these new properties to varying degrees into the thin film by varying the ratio of modified precursor to precursor ratio. In this project modified precursors such as methyltriethoxysilane(MTES) $CH_3Si(OC_2H_5)_3$, a derivative of TEOS and methyltrimethoxysilane (MTMS) $CH_3Si(CH_3)_3$, a derivative of TMOS were used.

2.6 Summary

This chapter introduced the sol-gel process and explained the parameters involved. By varying the parameters it is possible to vary film properties and tailor the film microstructure for specific purposes.

2.7 References

[1] L. Esquivias, J. Zarzycki; **Sonogels: An alternative Method in Sol-Gel Processing**, in J.D. Mackenzie and D.R. Ulrich, Eds., *Ultrastructure Processing of Advanced Ceramics*, Proc. Conf., Feb 23-27, 1987, San Diego, C.A., pp 255-270, Wiley, N.Y., 1988.

[2] C.J. Brinker, G.W. Scherer; Sol-Gel Science: **The Physics and Chemistry of Sol-Gel Processing**, Academic Press, San Diego, 1990, pp. 108.

[3] E.J. Pope, J.D. Mackenzie; **Sol-Gel Processing of silica: The Role of the Catalyst**, *J. Non-Cryst. Solids*, Vol. 87, pp. 185-188.

[4] E.R. Pohl, F.D. Osterholtz; **Molecular Characterisation of Composite Interfaces,** Plenium, (1985) pp 157.

[5] R.K. Iler; **The Chemistry of Silica**, Wiley (1979).

[6] I.M. Thomas; **Optical Coating Fabrication**, *Sol-Gel Optics: Processing and Applications*, Kluwer Academic Publishers, Ed L. C. Klein, 1994, pp. 141-158.

[7] C.M. McDonagh, F. Sheridan, T Butler, B.D. MacCraith; **Characterisation of Sol-Gel-Derived Silica Films**, *J. Non-Cry. Solids,* 1996, Vol. 194 pp. 72-77.

[8] S. Sakka; **The Current State of Sol-Gel Technology** *J. Sol-Gel Sci. Technol.* Vol.3 pp 369-381 (1994).

Chapter 3

Oxygen Sensing by Fluorescence Quenching

3.1 Introduction

The optical sensor used in this work is based on the collisional quenching by oxygen of a fluorophore entrapped in the sol-gel matrix. This chapter aims to introduce fluorescence, the fluorophore used and to explain how the fluorescence of the fluorophore is quenched in the presence of oxygen.

3.2 Fluorescence

When a fluorophore is irradiated with electromagnetic radiation, the energy of the incident photons can be transferred to the atoms or molecules raising them from the ground state. Luminescence is the emission of photons from these excited states. There are two types of luminescence, fluorescence and phosphorescence and these depend on the nature of the ground and excited states.

If the electron in the higher energy orbital has a spin orientation opposite to the electron in the lower energy level, the electrons are said to be paired. This is the singlet excited state. Fluorescence is the emission which results from a paired electron

returning to the lower orbital. This transition is quantum mechanically allowed and the emission rates are typically ~ 10^8 sec^{-1}[1].

A triplet state occurs when the electron in the excited state has the same spin as the electron in the ground state hence the electrons are unpaired. These transitions are quantum mechanically forbidden, emission rates are slow and the lifetime, τ is longer, where τ is the time spent in the excited state prior to fluorescence. Phosphorescence is the emission which results from these transitions between states of different multiplicity i.e. triplet to singlet ground state[2].

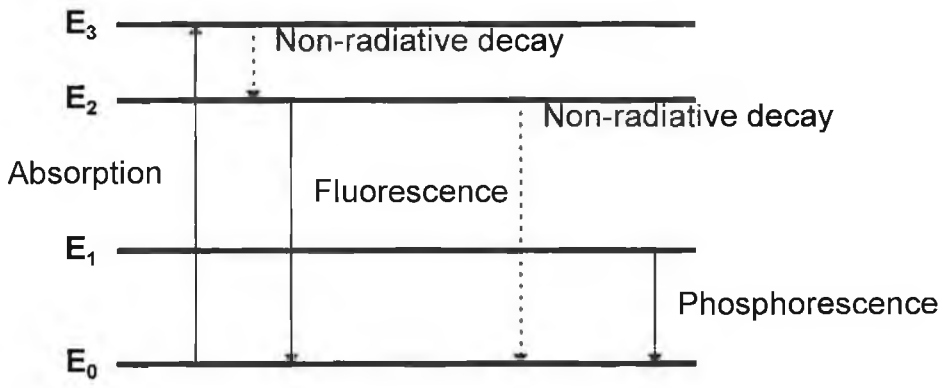

Figure 3.1 Basic Excitation and Emission Processes

Figure 3.1 shows a simplified energy level diagram for absorption and emission of light. In the diagram E_0 is the ground state, the singlet state is E_2 and the triplet state is E_1. If a molecule is excited by an incoming photon and is raised to excited state E_3, the absorbed energy can be released radiatively or non- radiatively. Generally the electrons will decay non-radiatively between E_3 and E_2, releasing heat into the surrounding material. Radiative decay will occur from the singlet state E_2 and the triplet state E_1. The fluorophore used in this work has a singlet ground state and a triplet emitting state.[3] This results in a partially allowed transition of relatively long lifetime. Where decay results in radiation, the emitted photons have energies:

$$h\nu_1 = E_1 - E_0 \qquad (3.1)$$

Strictly speaking this emission is phosphorescence as defined above but in this work it will be referred to as fluorescence.

3.3 Ruthenium Complexes

Fluorescent transition metal complexes are widely used in optical sensor applications[1,4]. This is due to the fact that they are highly fluorescent with long lifetimes and have high quantum yields (ratio of the number of photons emitted to those absorbed). These complexes have strong absorption in the blue green region of the spectrum which makes them compatible with laser and LED sources. The Stokes shift is the difference in wavelength between absorption and fluorescence maxima and for transition metal complexes this is relatively large. This enables the use of filters to allow the minimum excitation light to be detected with minimal reduction of fluorescence signal.

The complex used in this work is ruthenium (II)-tris(4,7-diphenyl-1,10-phenanthroline) $[Ru(II)(Ph_2Phen)_3]^{2+}$ This is an octahedral complex where the diphenylphenanthroline groups are bidentate ligands. This means that each ligand bonds to the central metal atom at two sites. Figure 3.2 shows the ligand and where it bonds to the metal atom through the nitrogen atoms a and b.

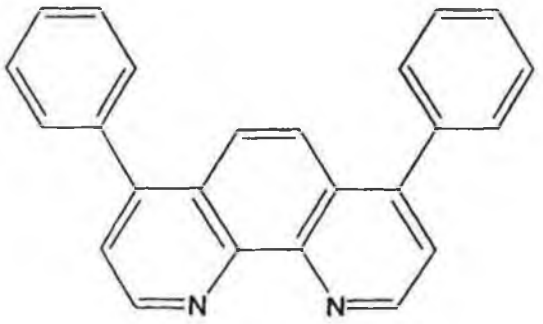

Figure3.2 Structure of the Diphenylphenanthroline Ligand

This ruthenium complex is a d^6 complex which means that it has a partially filled d orbital. The octahedral field of the ligand splits into five different levels, a doubly degenerate e_g level and a triply degenerate t_{2g} level[3]. There is an energy gap between these levels due to the crystal field splitting energy (CFSE),Δ. This is due to the negative field of the ligands acting on the electrons in the metal d orbitals. Figure 3.3 shows the orbitals of a transition metal ion in a ligand field.

Electrons occupying the d_{Z2} or d_{X2-y2} atomic orbitals will be repulsed to a greater extent than an electron occupying a d_{yz}, d_{xz} or d_{xy} atomic orbital. Figure 3.4 shows a simplified orbital diagram for a d^6 octahedral complex. The electrons will appear in either high or low spin energy states depending on the CFSE. The CFSE is determined by the crystal field strength of the ligands and the metal ion. When the CFSE is large all of the electrons will appear in the t_{2g} level and when the CFSE is small they will appear in both levels. This is because the energy gap between the levels is less that the energy required to pair the electrons in one energy level. The ruthenium complex used in this work has a large CFSE so that all the electrons appear in the t_{2g} level.

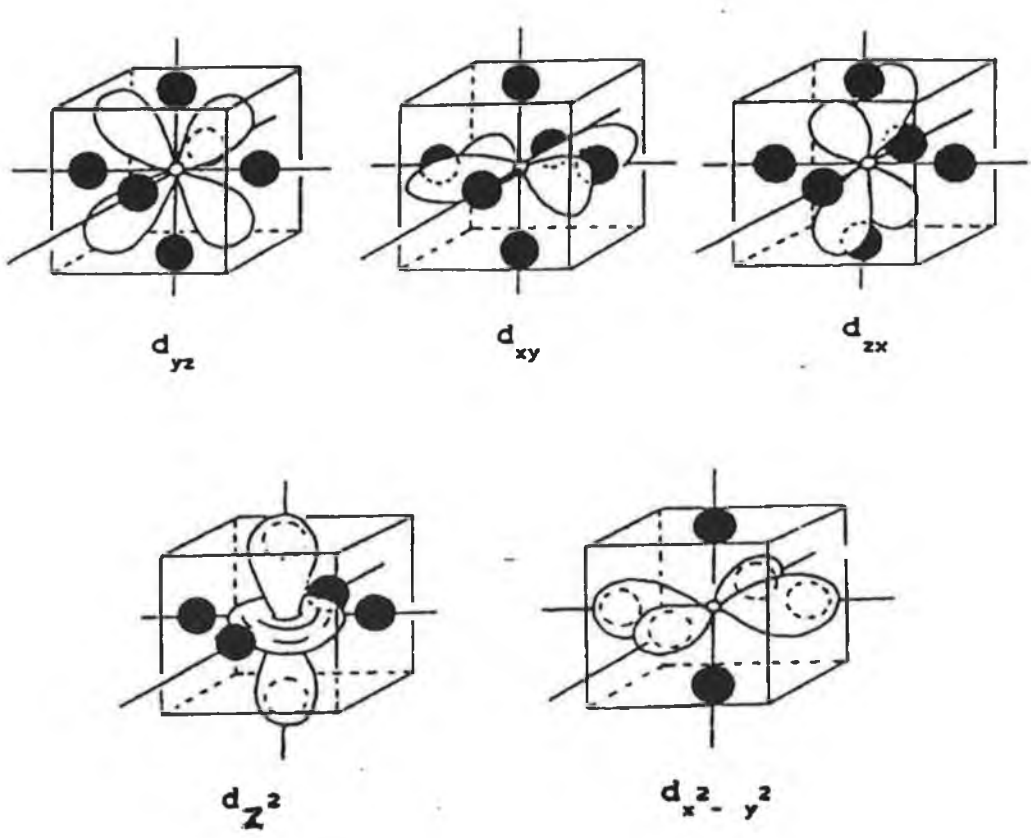

Figure 3.3 Orbitals of a Transition Metal Ion in a Ligand Field

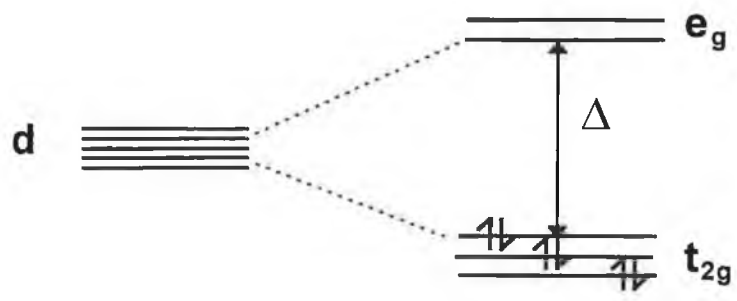

Figure 3.4 Simplified Orbital Diagram for Ru(II)tris(4,7-diphenyl-1,10-phenanthroline)

The ligands bonded to the metal atom have both σ and π orbitals. However only π orbitals are important for visible and near-ultra violet absorptions and emissions. π

orbitals can be either bonding (π) or antibonding (π^*) but only π bonding orbitals are filled. Since the complex is low spin and all electrons are paired, the ground state is a singlet state. When the complex absorbs light there are three types of excited states for an octahedral field

1. Where a d electron is promoted to another d level (a d-d transition).
2. Where a π bonding electron is promoted to a π^* antibonding level (a π-π^* state).
3. a. Metal to ligand charge transfer (MLCT) where a d electron is promoted to a π^* orbital

3.b. Ligand to metal charge transfer (LMCT) where an electron in a π bonding orbital is promoted to an unfilled d orbital.

For the ruthenium complex used in this work the MLCT excited state is the lowest in energy with respect to all other excited state transitions and so this is the main absorption transition. The absorption maximum occurs at 450 nm due to this and the Stokes-shifted emission of the MLCT excited state to the ground state gives a fluorescence maximum of 608 nm in aqueous solution and 611nm in sol-gel films[5]

3.4 Fluorescence Quenching by Oxygen

Any process which cause the non-radiative loss of energy from a molecule in the excited state is referred to as fluorescence quenching. There are two different ways that this can happen[2]:

1. Static Quenching refers to complex formation between the fluorophore and the quencher where the complex formed is non-fluorescent.

2. Collisional or Dynamic Quenching refers to non-radiative transfer of energy when a free molecule interacts with the fluorophore in the excited state.

In this work the fluorescence quenching is due to collisional quenching by molecular oxygen. The quencher (oxygen) diffuses to the fluorophore during the lifetime of the excited state, so the quenching is dependent on the concentration of the quenching molecule and on the rate at which the quencher can diffuse to the excited fluorophore. Quenching affects both the intensity and the lifetime of the fluorophore.

Quenching is governed by the Stern-Volmer equation[6]:

$$\frac{\tau_o}{\tau} = \frac{I_o}{I} = 1 + K_{sv}[Q] \qquad (3.2)$$

Where τ_o and τ are the lifetimes of the fluorophore in the absence and presence of quencher and I_o and I are the fluorescence intensities in the absence and presence of quencher. [Q] is the concentration of quencher and Ksv is the Stern-Volmer quenching constant:

$$Ksv = k\tau_o \qquad (3.3)$$

Where k is the bimolecular quenching constant which is proportional to the oxygen solubility of the matrix and the diffusion coefficient of oxygen in the sol-gel film.

Theoretically a Stern-Volmer plot of I_o/I or τ_o/τ against quenching concentration, will give a straight line graph of slope Ksv and intercept of 1 on the y axis. However in the work carried out for this project the Stern-Volmer plot deviates from linearity due to the inhomogenety of the fluorophore environment[3].

3.5 Fluorescence Decay Times

The decay time or lifetime of the excited state is defined as the average time the fluorophore spends in the excited state prior to returning to the ground state. The observed lifetime depends on the radiative and non-radiative decay rates as shown in equation 3.4,

$$K_{obs} = \frac{1}{\tau} = \frac{1}{\tau r} + \frac{1}{\tau nr} \qquad (3.4)$$

where $1/\tau$ is the observed decay rate, K and where r and nr refer to the radiative and non-radiative lifetimes respectively.

Fluorescence decay time measurements offer a number of advantages over fluorescence intensity measurements for optical sensing [7]:

- Decay times are absolute quantities and are usually independent of light source stability.
- Decay time is independent of fluorophore concentration, so there is no signal drift due to photobleaching or leaching.

There are two methods which are widely used to measure fluorescence decay times:

1. Pulse method:

   The sample is excited by a brief pulse of light and the time dependent decay of fluorescence intensity is measured.

2. Phase modulation method:

   The sample is excited with sinusoidally modulated light. The phase shift and demodulation of emission relative to the incident light is used to calculate the decay time.

In this project the pulse method is used. This is dealt with in section 4.6.

In an ideal situation the decay time of the fluorophore will follow a single exponential decay. The time dependence of the decay is given by:

$$I = I_o e^{-kt} \qquad \textbf{(3.5)}$$

where I_o is the maximum intensity and k, the decay rate constant equals τ^{-1}. So the decay time can be measured as the time taken for the emitted radiation to fall to 1/ e of its original intensity. This equation can be rewritten as:

$$\ln I = \ln I_o - kt \qquad \textbf{(3.6)}$$

A plot of ln I against t will have a slope of - k from which the lifetime can be calculated.

When the fluorophore is entrapped in the sol-gel matrix it will exist in a range of fluorescence sites due to the amorphous nature of the glass film. This gives rise to a distribution of decay times resulting in a non-exponential measured decay. For a small degree of non-exponentiality, it is sometimes convenient to analyse the data as a sum of two exponential decays, although the two decays may not have any physical significance. In this project best fits were obtained from either single exponential or double exponential decays. Various decay time analysis methods are discussed in section 4.6

3.6 Summary

This chapter introduced fluorescence, fluorescence quenching and fluorescence decay times. The fluorophore used is a ruthenium complex with a singlet ground state and a triplet excited state. It absorbs at 450nm and has a fluorescence maximum at 611nm in the sol-gel matrix. The fluorescence is quenched by collisional quenching by oxygen.

3.7 References

[1] J.N. Demas, B.A. Degraff; **Design and Applications of Highly Luminescent Transition Metal Complexes**, *Anal. Chem.*, 1991, Vol. 63, No. 17, pp. 829.

[2] J.R. Lakowicz; **Principles of Fluorescence Spectroscopy**, Plenum Press 1993.

[3] A.K. McEvoy; **Development of an optical Sol-Gel Based Dissolved Oxygen Sensor**, PhD. Thesis, 1996, Dublin City University (unpublished).

[4] B.D .MacCraith, G O'Keeffe, A.K. McEvoy, C.M. McDonagh: **Development of a LED-based Fibre-optic oxygen sensor using sol-gel-derived coatings,** *Proc. SPIE*, 1994, Vol. 2293, pp.110.

[5] K.F. Mongey, J.G. Vos, B.D. MacCraith, C.M. McDonagh, C. Coates, J.J. McGarvey; **Photophysics of mixed ligand polypyridyl ruthenium (II) complexes immobilised in silica sol-gel monoliths**, *J. Mater. Chem.*, 1997, Vol. 7 No. 8 pp 1473-1479.

[6] O Stern, M. Volmer, *Z. Physic*, 1919, Vol. 20, pp. 183.

[7] P.F. Kiernan; **Oxygen Sensitivity of Ruthenium- Doped Sol-Gel- Derived Silica Films**, M.Sc. Thesis, 1994 (unpublished).

Chapter 4

Experimental Techniques

4.1 Introduction

Chapter 2 deals with the theory of the sol-gel process. This chapter details the methods used to fabricate the sol-gel thin films. By varying parameters it is possible to vary the film properties. Section 4.2 details the different parameters that are varied and the effect that this has on sensor properties is looked at in subsequent chapters. The methods of characterisation are described which include thickness and hydrophobicity measurements, fluorescence quenching and fluorescence lifetime analysis.

4.2 Film Fabrication

For this project films were fabricated from tetraethoxysilane (TEOS) and related organically modified precursors, methlytriethoxysilane (MTES) and ethyltriethoxysilane (ETES) and also from tetramethoxysilane (TMOS) and related precursors, methyltrimethoxysilane (MTMS) and ethyltrimethoxysilane (ETMS). Films fabricated using organically modified precursors are termed ormosils (organically modified silicates).

4.2.1 Sol Fabrication

Sols were fabricated using alkoxysilane, solvent and deionised water of required pH with hydrochloric acid as a catalyst.

4.2.1.1 TEOS and Related Ormosil Films

For doped sols 40,000 ppm of ruthenium complex (based on amount of Si) was measured into a clean glass vial and dissolved in ethanol. Water of required pH and corresponding to the desired R value (i.e. water: precursor ratio, section 2.3.2), was measured into the solution and mixed to induce homogeneity, since alkoxysilanes are not miscible with water. The TEOS based precursors were added dropwise while mixing. The sol was left to mix for one hour. TEOS sols were left to age for 18 hours at 70°C to induce hydrolysis and condensation. Ormosil films did not require ageing and were dip-coated onto substrates after mixing.

4.2.1.2 TMOS and Related Ormosil Films

TMOS based sols were fabricated with methanol as a solvent. The reason that methanol as opposed to ethanol was used for these sols is that during the course of the hydrolysis reactions when an ethoxy group is hydrolysed (as in TEOS) ethanol is evolved from the reaction (see section 2.1). When a methoxy group is hydrolysed as in TMOS methanol is evolved in the reaction. So to keep the solvent consistent in both TEOS and TMOS sols, ethanol was used for TEOS sols and methanol was used for TMOS sols.

40,000 ppm of ruthenium complex was dissolved in methanol and the precursor was added to this. Solvent and precursor were left to mix for 10 minutes to induce homogeneity and then the deionised water was added dropwise. TMOS sols hydrolyse

much faster than TEOS sols due to less steric hindrance, as discussed in section 2.2, and so no ageing was required. All sols were dip-coated after one hour of stirring.

4.2.2 Film Fabrication parameters

4.2.2.1 Precursor

The aim of this project is to fabricate and characterise sol-gel sensor films. In order to do this the effect of precursor on film properties is investigated. Section 2.5 outlines the effect that organically modified precursors can have on film structure. TEOS and MTES were mixed in different ratios and the effect of the amount of MTES present investigated.

TEOS and TMOS based precursors have different hydrolysis and condensation rates due to steric hindrance (discussed in section 2.2). The effect of this on film characteristics was investigated and the results shown in the following chapters.

4.2.2.2 pH

Films were fabricated using water of pH=1. This gives rise to acid catalysed films. The effect of using water of different pH values was investigated. MTES films were made up using water of pH 2.5 and 4 , these films are base catalysed and their film properties compared to pH=1 films

4.2.2.3 R- value

The water to precursor ratio, R, greatly influences the structure of the film [1,2]. For this project films were generally made up at R=2, however R=4 films were also investigated and the results compared.

4.2.2.4 Ultrasound

The standard process for making sols in this laboratory involves magnetically stirring the sols for 1 hour prior to dipcoating in order to allow for hydrolysis and condensation reactions to occur. Ultrasound was investigated to see the effect on film properties.

When a sol is exposed to ultrasonic radiation there are two phases. In the low-pressure phase of the ultrasonic wave a cavity is formed, this cavity expands quasi-isothermally and becomes filled with solvent and solute vapours. During the high pressure phase the cavity suddenly collapses adiabatically leading to dramatic temperature increases (local hot spot temperature increases of up to several thousand degrees have been reported)[3]. It is at this point that reactions take place in the bubble. It is thought that water containing solutions involve the production of radicals by the thermal decomposition of water[4].

Since the use of ultrasound influences the reaction, sonogels are thought to have different microstructures to conventional gels for example smaller pores[3]. For this experiment sols were placed in an ultrasound bath, Ultrawave U50, for 15 minutes and the effect of this on film properties was investigated.

4.3 Film Thickness Measurements

Two methods were used to measure film thickness, ellipsometry and a spectral transmission technique.

4.3.1 Ellipsometry

Ellipsometry measures the difference in polarisation of a beam of light before and after it travels through a sample film and relates this to the thickness and refractive index of the film. Measurements were performed on a Rudolph Research AutoEL III ellipsometer. Figure 4.1 shows a schematic diagram of the ellipsometer. It is made up of a laser, polariser, analyser, compensator and detector. A collimated monochromatic beam from the helium neon laser is passed through the variable polariser so that the polarisation is known and controlled. The light is incident on the sample film at an angle of 70°. On travelling through the film the beam is reflected and passed through the analyser and on to the photodetector. Since the beam has passed through the sample, the polarisation of the beam has been modified.

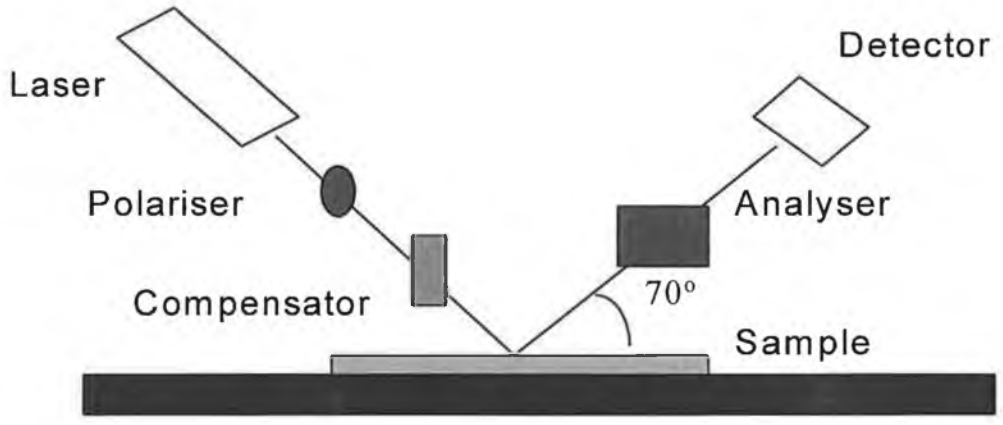

Figure 4.1 Schematic of the Ellipsometer

The polarisar and the analyser are rotated alternately until the intensity of the beam is reduced to a minimum. The angles of the polariser and analyser are then determined. These angles are converted by linear equations[5] into the parameters Δ and Ψ. These

parameters are functions of the incident angle, the thickness of the thin film and the refractive indexes of the surrounding medium, substrate and thin film. Since some of these parameters are known, the ellipsometer's software can determine the sample thickness and refractive index.

Δ and Ψ are cyclic functions of the film thickness which means that when the optical path length (refractive index times the physical path length) of the light traversing the film reaches an integer number of times the wavelength, it gives a reading as for no film at all. The ellipsometer gives readings of the full cycle thickness, S, the zero order thickness, T and the refractive index of the film. The actual thickness of the film can be

T, T+S, T+2(S),.....etc.

Hence it is necessary to have an independent method of measuring the film thickness. For this project data obtained from spectral transmission was also used to measure film thickness.

4.3.2 Spectral Transmission

The thickness of sol-gel films can be determined by measuring the transmission spectra on a UV/VIS spectrophotometer[6]. The transmission spectra are obtained from thin films coated on to both sides of a glass substrate run on a spectrophotometer over the wavelength range 200 - 1100nm. This method is based on a non-absorbing coating and the thickness can be determined from the position of the interference maxima/ minima[7].

The basic condition for interference fringes when light is passed through a thin film is

$$2 n d = m \lambda \qquad \textbf{(4.1)}$$

Where d is the thickness of the film, n is the refractive index of the thin film, m is the fringe number and λ is the wavelength of light.

From this it follows that the thickness can be given by:

$$d = \frac{\Delta m}{2n_c[1/\lambda_1 - 1/\lambda_2]} \qquad \textbf{(4.2)}$$

n_c is the refractive index of the coating, Δm is the order of separation of the peaks and λ_1 and λ_2 are the wavelength positions of the peaks. These parameters can be seen in figure 4.2

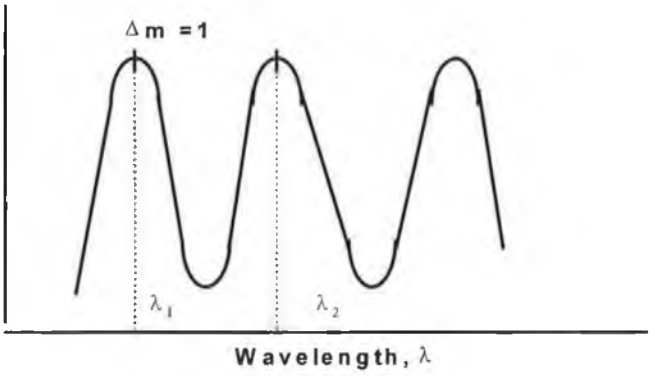

Figure 4.2 Interference Fringes.

This method of determining thickness is limited to cases where the front film is identical to the back film and also the films need to be thicker than 300 nm. Errors can occur because the refractive index of the film and the glass substrate are quite close, so the peaks transmission values are closely separated and broadness of the peaks introduces uncertainty in determining the exact wavelength positions of extrema.

Thickness measurements obtained from ellipsometry and from spectral transmission data do not agree exactly because sol-gel films are generally 5-15% thicker on glass substrates than on silicon [7]. Data from spectral transmission is a good method when

used in conjunction with ellipsometry, to determine how many times the zero order thickness should be added.

4.4 Hydrophobicity Measurements

The hydrophobicity of the sol-gel film is a crucial parameter for the use of films in a dissolved oxygen sensor Two methods where used to look at the hydrophobicity of the films, FTIR and contact angle measurements.

4.4.1 FTIR

Fourier transform infrared spectroscopy [FTIR] has proven a useful tool for studying the structure of sol-gel derived silica glasses [8,9,10,]. Molecular vibrations absorb in the infrared part of the spectrum. Hence infrared absorption data can be used to identify species such as Si-OH (silanol groups) in films. The hydrophobicity of sol-gel films can be investigated by looking at a wide band ~ 3400 cm^{-1} which is due to -OH stretching. For hydrophobic films this band is reduced compared to hydrophilic films.

For this project a Bomem MB 120 FTIR spectrometer was used scanning from 4000 - 400 cm^{-1} and all the main features were assigned. All spectra are a result of 50 scans at normal incidence with a resolution of 4 cm^{-1}. Films were coated onto silicon substrates and a baseline from an uncoated silicon slide subtracted.

4.4.2 Contact Angle

The contact angle of a solid with respect to a liquid (water in this case) is the angle between the tangent to the point of contact at the solid/ liquid/ vapour interface and the substrate plane (figure 4.2). The smaller the angle, the more easily the liquid is spread over or adheres to the solid surface, this is shown in figure 4.3 (a). When the contact angle reaches zero, the solid is completely wet. This would be characteristic of highly hydrophilic films. For contact angles greater than 90° the liquid does not wet the surface at all, as seen in figure 4.3(b)[11].

Figure 4.3 Contact Angles for hydrophilic, (a) and hydrophobic, (b) solid surfaces

The hydrophobic measurement apparatus uses the Wilhelmy plate technique to measure the dynamic contact angle of the sol-gel films. The Wilhelmy plate technique was first proposed in 1863 and advanced by the use of Young's equation in 1906 [12]. The system is home-made and shown in figure 4.4. The sample is held suspended from a movable stage which is operated by a stepper motor and controlled by a computer. The sample is dipped in and out of the liquid which is held on an electrobalance. This measures the force that is exerted by the interaction of the liquid and solid surface. The data is collected by the computer and is depicted by a Wilhelmy plate hysteresis loop shown in figure 4.5.

Contact angle hysteresis is the difference between advancing and receding contact angles. The most common sources of hysteresis are due to surface roughness and surface heterogeneity [13]. For an ideal surface wet by a pure liquid, contact angle theory predicts one thermodynamically stable contact angle. In practice an ideal surface is rarely found and so the advancing and receding angles differ.

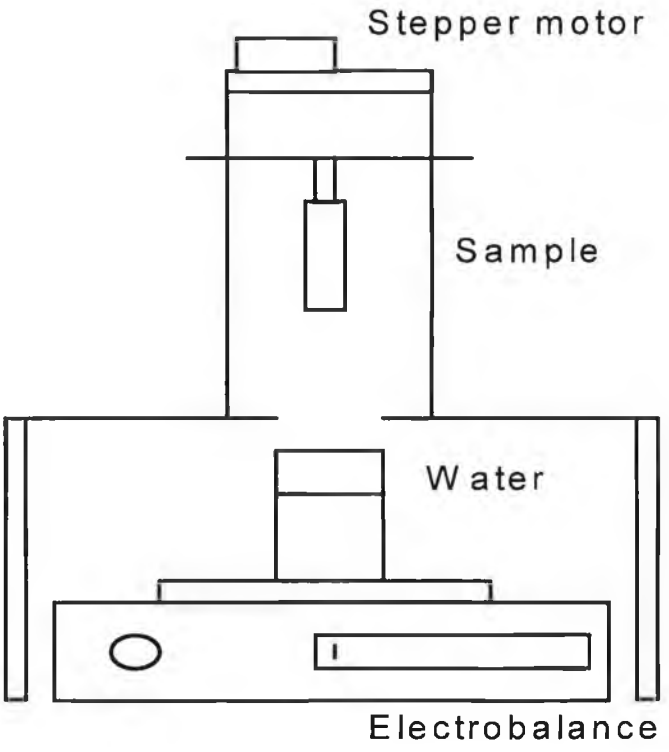

Figure 4.4 Contact Angle Apparatus

The advancing and receding contact angles are calculated from the hysteresis graph using a derivative of Young's equation[14]:

$$\text{Cos}\,\theta = F\,p\,\gamma \qquad \textbf{(4.3)}$$

where θ is the contact angle, F is the force measured from the hysteresis loop, p is the perimeter of the sample and γ is the surface tension of the liquid. For deionised water $\gamma = 0.061\ \text{Nm}^{-1}$. The contact angle assigned to the surface θ_{eqm} is the average of the

advancing and receding angles. The advancing or receding forces are taken from the hysteresis graphs where a straight line is fitted at the top and bottom of the hysteresis loop. This line is extrapolated to the zero depth line and F is read off the y axis. For this project contact angle measurements were carried out on sol-gel films coated on to glass substrates.

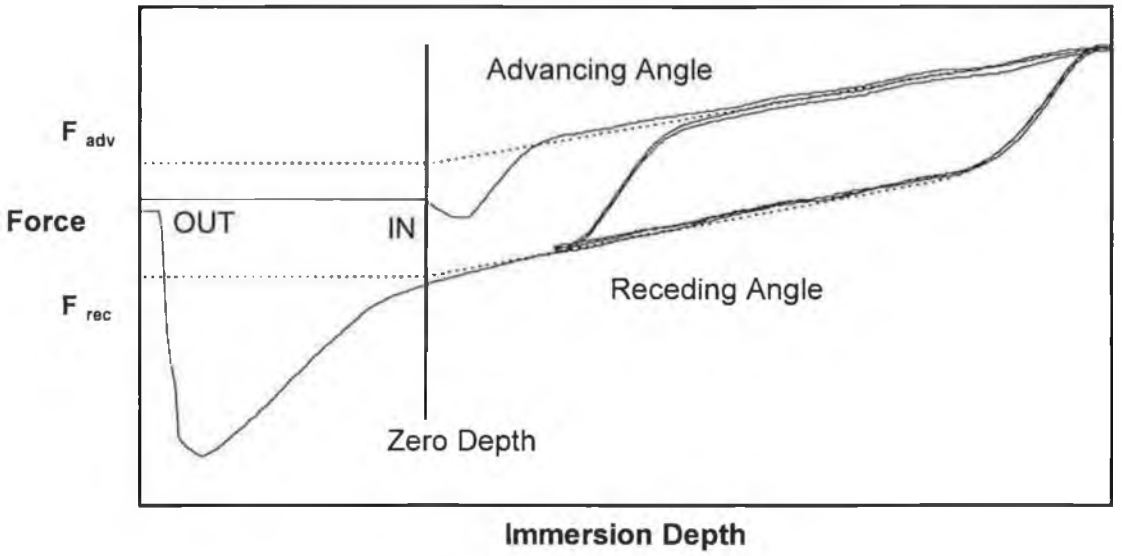

Figure 4.5 Wilhelmy Plate Hysteresis Loop

4.5 Fluorescence Quenching Measurements

Fluorescence quenching measurements were performed on the characterisation system shown in figure 4.6. The doped sol-gel coated glass slide is held in a sealed sample chamber. A high intensity blue LED is used as an excitation source for the ruthenium complex. Figure 4.7 shows the spectral output for the LED which is at 470nm and has considerable overlap with the absorption spectrum of the ruthenium complex.

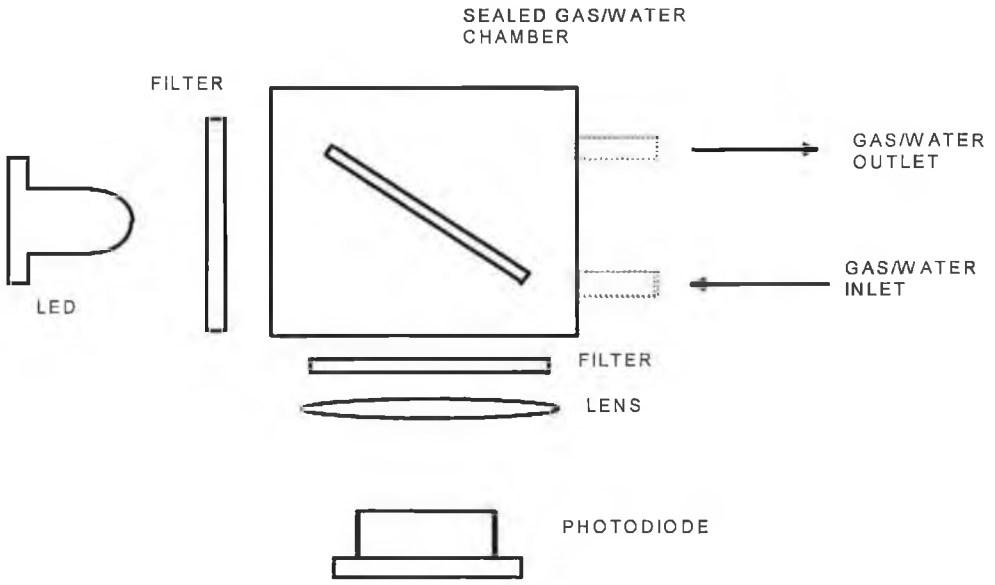

Figure 4.6 Characterisation System

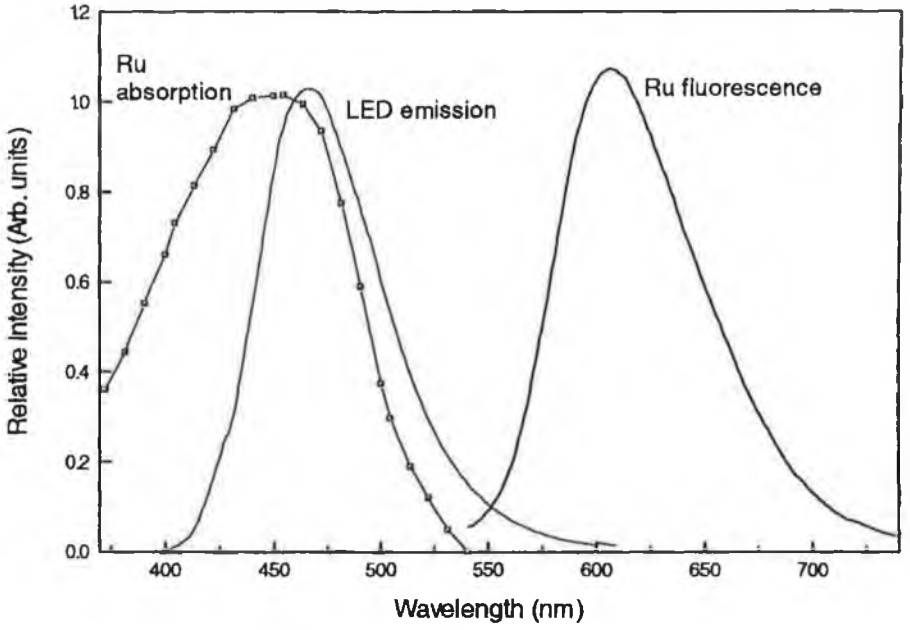

Figure 4.7 Overlap between absorption spectrum of the ruthenium complex and the emission spectrum of the LED

The light from the LED is passed through a wide-band pass filter, 400 - 505 nm (infrared Engineering, Maldon, Essex, UK) and is directed at the sample which is held at 45° to the LED beam. The fluorescence from the sample passes through a long-wave pass filter, $\lambda_{cut\text{-}on}$ = 570nm (CVI Laser Corporation, Albuquerque, N.M., USA) and is focused by a lens onto a photodiode detector (Hamamatsu, model S1223-01). The data from the system is digitised and passed to a PC for analysis and display.

Gas phase measurements were obtained by flowing oxygen and nitrogen into the sample cell via mass flow controllers.

100% humidified gas phase measurements were performed by flowing the gases through four water filled gas bottles and then to the sample cell.

Aqueous phase measurements were performed by bubbling oxygen or nitrogen into a sealed reservoir of deionised water while continuously stirring and then pumping the water via a peristaltic pump into the sample cell.

4.6 Fluorescence Lifetime Measurements

Fluorescence lifetime analysis was performed on the system shown in figure 4.8. The doped sol-gel coated glass slide is excited using 15ns pulses from a frequency-doubled Nd-YAG laser (λ= 532nm). To avoid photobleaching of the samples, neutral density filters were used to cut down the intensity of the excitation radiation. The fluorescence from the sample is collected and focused using lenses, onto the slits of a Jobin- Yvon one meter spectrometer set at 610nm. The spectrometer is essentially working as a filter. The fluorescence is collected using a Hamamatsu photomultiplier tube. The data is displayed on an oscilloscope (HEWLETT-PACKARD 54600A

digital storage scope) with an input impedance of 50 Ohms. The oscilloscope allows for signal averaging and storage before the data is passed to a PC to be processed.

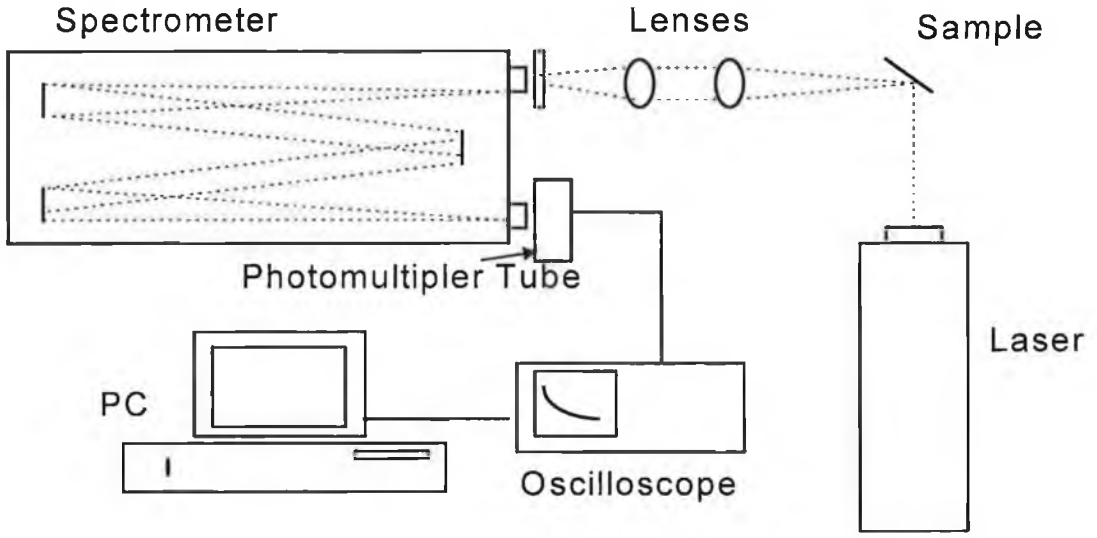

Figure 4.8 Lifetime Measurement Set-up

4.6.1 Data Analysis

The fluorescence lifetime of the ruthenium complex entrapped in the sol-gel films was investigated both in air and also in 100% nitrogen. As mentioned in section 3.4, due to the amorphous nature of the glass films, there is a distribution of decay times which can result in a non-exponential measured decay. Sometimes it is possible to fit this to a double exponential decay. For this project decay curves were fit to either single exponential or double exponential decay curves using a graphing package called Origin. An alternative method of characterising non-exponential decay curves is to define an average lifetime τ_{av}. This method measures the area under the decay curve as follows:

$$\tau_{avg} = \frac{\sum_{i=1}^{n} t_i I_i(t)}{\sum_{i=1}^{n} I_i(t)} \qquad (4.4)$$

where I is intensity and t is time.

4.7 Summary

This chapter outlined the method of fabrication for the sol-gel thin films. Different parameters are varied for this work and these are outlined in section 4.2. The effect of varying parameters has an effect on film properties and so the films are characterised using different techniques. These techniques were detailed in this chapter.

4.8 References

[1] A.K. McEvoy; **Development of an Optical Sol-Gel Based Dissolved Oxygen Sensor**, PhD. Thesis, 1996, Dublin City University (unpublished)

[2] C.M. McDonagh, F.R. Sheridan, T. Butler, B.D. MacCraith; **Characterisation of Sol-Gel-Derived Silica Films**, *J. Non-Crys. Solids*, 1996, Vol. 194, pp. 72-77

[3] L. Esquivias, J. Zarzycki; **Sonogels: An Alternative Method in Sol-Gel Processing**, in: J.D. Mackenzie and D.R. Ulrich, Eds., *Ultrastructure Processing of Advanced Ceramics*, Proc. Conf. Feb 23-27, 1987, San Diego, C.A., pp 255-270, Wiley, N.Y., 1988

[4] J. Zarzycki; **Sonogels: Development and Perspectives**, in D. R. Uhlmann and D. R. Ulrich, Eds., *Ultrastructure Processing of Advanced Materials*, pp 135-148, Wiley, N.Y., 1992

[5] Rudolph Research AutoEL-III Ellipsometer, **Condensed Operating Instructions**.

[6] O.S. Heavens: **Optical Properties of Thin Solid Films**, Dover Publications, New York (1965).

[7] V.J. Murphy; **Quasi-Distributed Fibre-Optic Chemical Sensing Using Telecom Fibre**, MSc. Thesis,1997, Dublin City University (unpublished).

[8] R.M. Almeida, H.C. Vasconcelos; **Relationship Between Infrared Absorption and Porosity in Silica Based Sol-Gel Films**, *Proc. SPIE* , 1994, Vol. 2288, pp. 678-687

[9] P. Innocenzi, M.O. Abdirashid, M. Guglielmi; **Structure and Properties of Sol-Gel Coatings from Methlytriethoxysilane and Tetraethoxysilane**, *J. Sol-Gel Sci. Technol.*, 1994, Vol.3, pp. 47-55

[10] L. Yang, S. Saavedra, N.R. Armstrong, J. Hayes; **Fabrication and Characterisation of Low-Loss, Sol-Gel Planar Waveguides**, *Anal. Chem.*, 1994, Vol.66:8, pp. 1254-1263.

[11] G.A. Somorjai; **Introduction to Surface Chemistry and Catalysis**, Wiley, Interscience pp. 296.

[12] Cahn Dynamic Contact Angle Analysis, Operators Manual.

[13] J.D. Andrade; **The Contact Angle and Interface Energies, Surface and Interfacial Aspects of Biomedical Polymers**, 1985, Vol 1 Plenium Press, N.Y.

[14] G. Aichmayr; **Measurement of Surface Tension**, Degree in Applied Physics Final Year Report, Dublin City University (unpublished).

Chapter 5

Film Thickness and Stabilisation

5.1 Introduction

This chapter looks at work carried out on thickness behaviour of sol-gel thin films. Past work is summarised and followed by the results of the studies carried out for this project. All thickness measurements were taken from an average of six measurements with a standard deviation of 20nm.

5.2 Theoretical Behaviour and Previous Studies

Studies have been carried out on the effect of various parameters on film thickness. In this section, the results of previous studies as well as theoretical behaviour will be reported in order to give a background on the parameters that were varied for this project.

5.2.1 Effect of Coating Rate on Film Thickness

The relationship between coating rate and film thickness for dip coating is given in equation 5.1[1].

$$\text{thickness} \propto \left[\frac{(\text{viscosity})(\text{withdrawal speed})}{\text{liquid density}}\right]^{2/3} \qquad \textbf{(5.1)}$$

If the viscosity and the density of the sol remain constant this relationship can be given by equation 5.2

$$\text{thickness} \propto [\text{withdrawal speed}]^{2/3} \qquad \textbf{(5.2)}$$

The above equation predicts a power dependence of 0.66 but this can vary between 0.5 and 0.7 depending on assumptions related to surface tension and viscosity. Studies were carried out on TEOS films with R values of 2, 4, 6 and 7 (made with pH=1 water)[2]. It was found that films with R values of 4, 6 and 7 agreed with theory whereby a plot of log(thickness) verses log(coating rate), gives a slope between 0.5 and 0.65. Films of R=2 deviated from this and gave a slope of 0.4. It was concluded that R=2 films deviated from theory due to the relatively small amount of water present thus reducing the hydrolysis and condensation reactions. This behaviour of TEOS R=2 films is consistent with other anomalous results found as described below.

5.2.2 Effect of Ageing Time on Film Thickness

Ageing or prepolymerisation of the sol causes aggregation due to hydrolysis and condensation reactions. Sols are generally left to age if they do not coat the substrate immediately after dipping. If a sol is left to age for too long, the sol will gel before coating. Work carried out has found that when the coating rate is fixed the film thickness increases with ageing time but this rate of increase is slower for R=2 films[3].

5.2.3 Effect of Drying on Film Thickness

A study of drying time on film thickness was carried out[3]. Drying time was varied between 1 and 120 hours at 100°C for TEOS R=2 films. It was found that while increasing drying time did reduce the initial thickness of the film, all films regardless of drying time had virtually the same thickness when stabilised.

5.2.4 Summary

In light of the findings described above, all films for this project were coated at a constant rate of 1mm/sec. Ageing times and drying times were varied for different precursors as described below and films, where appropriate were doped with the ruthenium complex $Ru(II)[(Ph_2Phen)_3]^{2+}$.

5.3 Temporal Behaviour of TEOS and MTES Films

Films were fabricated using TEOS and MTES in different molar ratios at R=2 and with water of pH=1 without addition of the dye complex. TEOS sols will not coat immediately after stirring and so they were aged at 70°C for 18 hours prior to dip coating. This ageing time is designed to produce films of thickness ~ 450nm. Hydrolysis and condensation rates for MTES films are faster than for TEOS and this is reflected in the sol coating the substrate immediately after stirring. However when these films are put into the oven to dry at 70°C, the films seem to 'evaporate' off. When these films are left to dry at room temperature for one week, the films are of good quality. MTES:TEOS mixtures give good quality films that do not require ageing and can be dried at 70°C for 18 hours.

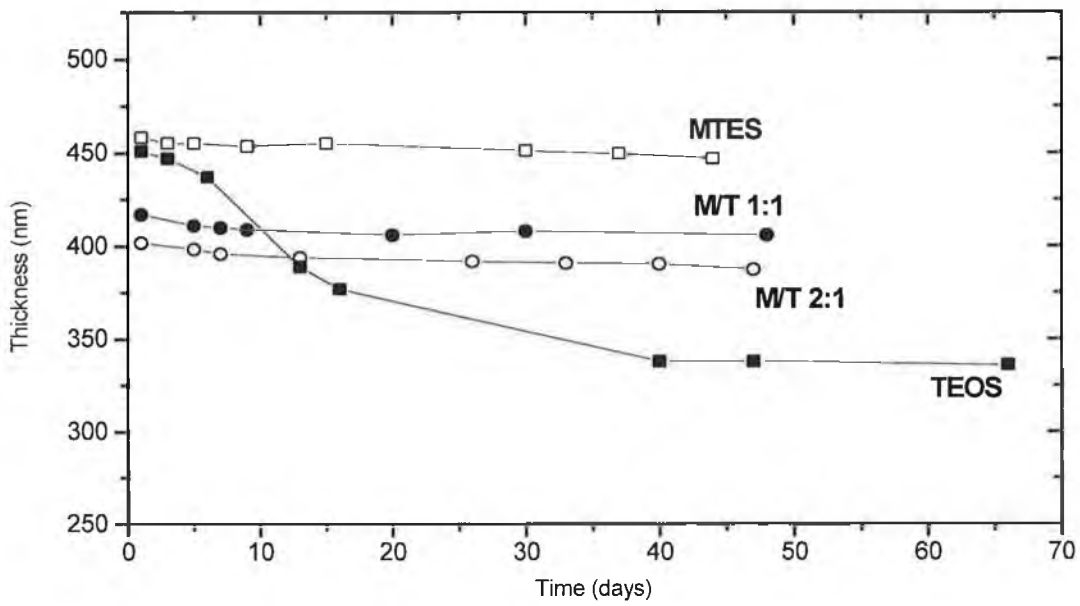

Figure 5.1 Thickness verses Time for R=2 pH=1 Films

Figure 5.1 shows the results of the study. TEOS films take up to 40 days for thickness stabilisation, whereas MTES films are stable within a few days. The mixtures of MTES:TEOS 1:1 and 2:1 both stabilised between 7 and 9 days. MTES sols have faster hydrolysis rates compared to TEOS and this is reflected in the stabilisation rates for the films. The mixtures of MTES:TEOS take longer to stabilise than MTES due to the presence of TEOS in the sols. Although R=2 is the stoichiometric water: TEOS ratio, complete hydrolysis does not take place It can be seen from the literature that even at high R values, unhydrolysed monomers can still remain in the gel[4]. The result of this incomplete hydrolysis prior to coating results in continuing hydrolysis taking place in the film facilitated by exposure to moisture in the atmosphere, which is reflected in a gradual decrease in film thickness over time for TEOS films.

5.4 Effect of Dopant on Film Thickness

For this study films were fabricated from TEOS, MTES and a 1:1 ratio TEOS:MTES. All films had 2.5 g/l of the ruthenium complex Ru(II)$[(Ph_2Phen)_3]^{2+}$ incorporated into the sol-gel matrix From the previous section, when MTES R=2 films are fabricated with no ruthenium they cannot be dried at 70°C while maintaining film quality. However doped MTES films are of better quality and are able to withstand drying at 70°C.

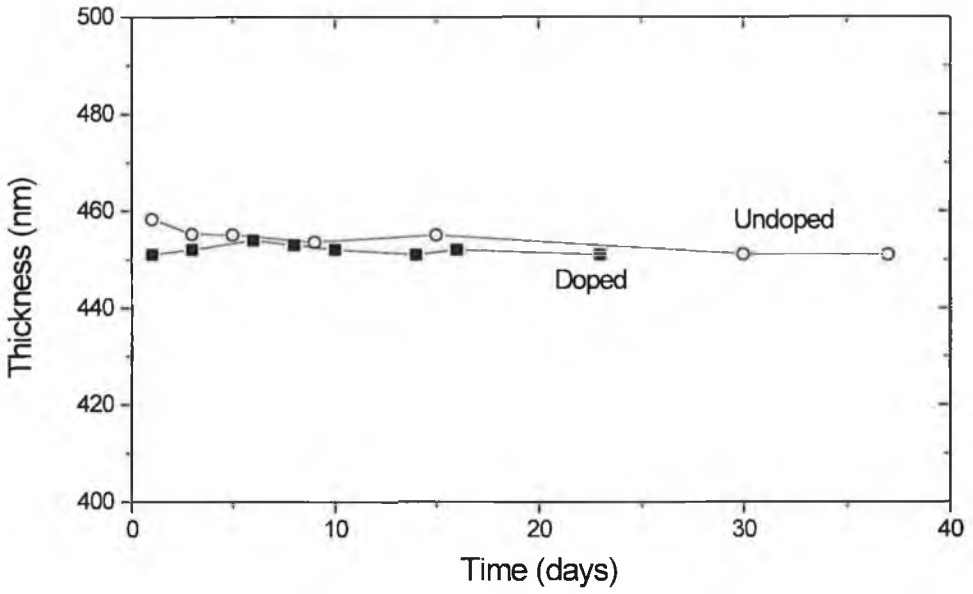

Figure 5.2 MTES Doped and Undoped Films

From figure 5.2 it can be seen that MTES films doped and undoped give the same film thickness within the 20nm error.

MTES:TEOS 1:1 doped films are stable immediately after drying as for MTES. It can be seen from figure 5.3 that undoped films take longer to stabilise and are not as thick as doped films, the difference in thickness being ~25nm. Figure 5.4 shows the effect

of dopant on TEOS films. Doped TEOS films are initially thinner than undoped films although this is within the 20nm error, however undoped films stabilise to be thinner than doped films which is consistent with the smaller thickness found in figure 5.3 for mixed MTES:TEOS.

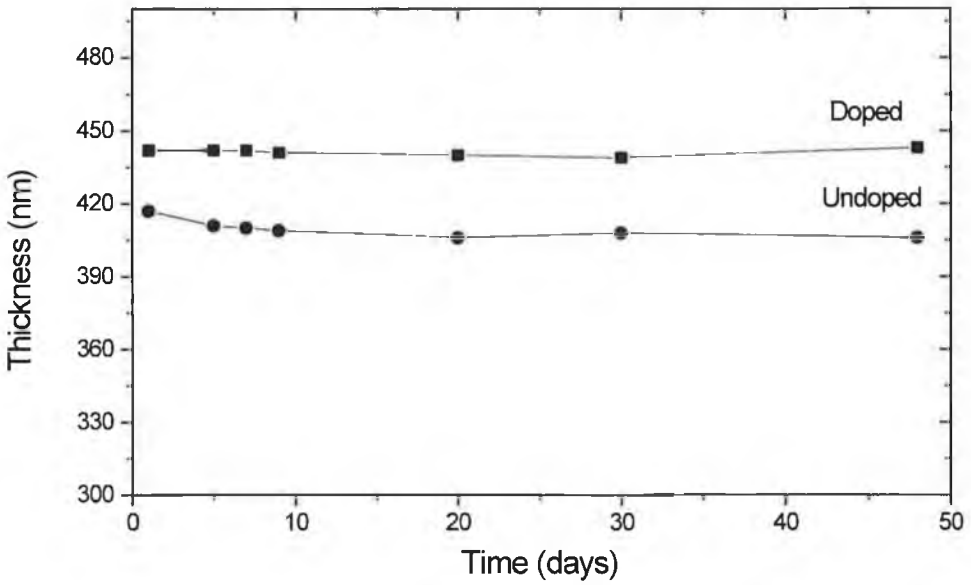

Figure 5.3 MTES:TEOS 1:1 Doped and Undoped Films

Similar thickness for doped and undoped MTES films compared to the thickness difference found in TEOS films and mixed TEOS:MTES films are consistent with the more flexible microstructure of MTES which incorporates the dye molecule in the matrix without an expansion in structure. TEOS on the other hand has a more rigid microstructure and the entrapped dye causes the film to expand giving an increased thickness.

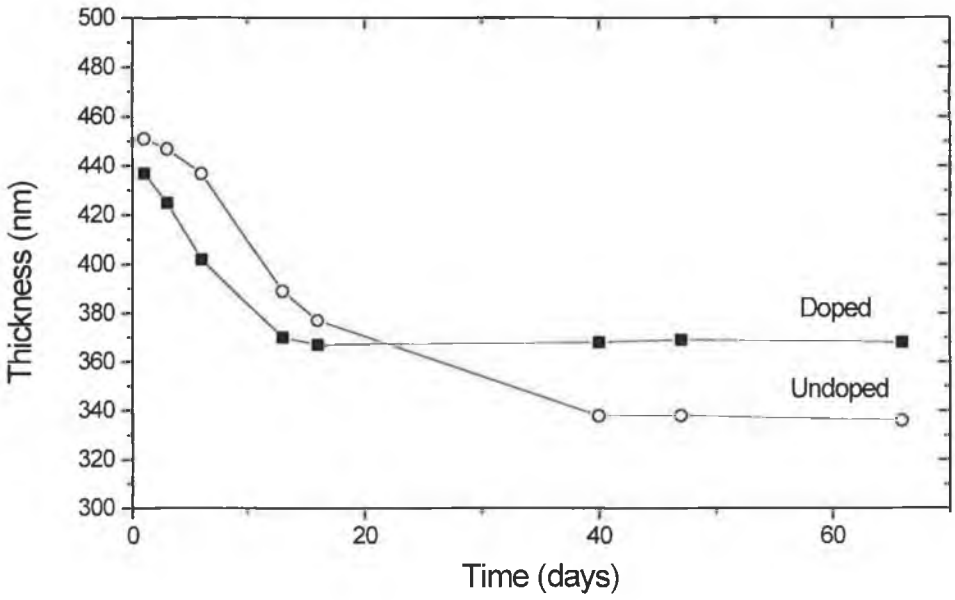

Figure 5.4 TEOS Doped and Undoped Films

It can be seen from figure 5.4 that the introduction of a dopant reduces thickness stabilisation time from over 40 days to less than 18 days.

The effects of introducing a dopant into the sol is assumed to cause an enhancement of the hydrolysis rate by the dye although the exact mechanism is as yet unknown.

5.5 TMOS and Related Ormosil Films

It has been reported that the hydrolysis and condensation rates for TMOS are significantly greater than for TEOS[4]. This is due to decreased steric hindrance for the TMOS molecule. All films fabricated for this study were doped with the ruthenium complex. Figure 5.5 shows that TEOS takes longer to stabilise than the other three and this is consistant with the longer gel time of TEOS compared to the others.

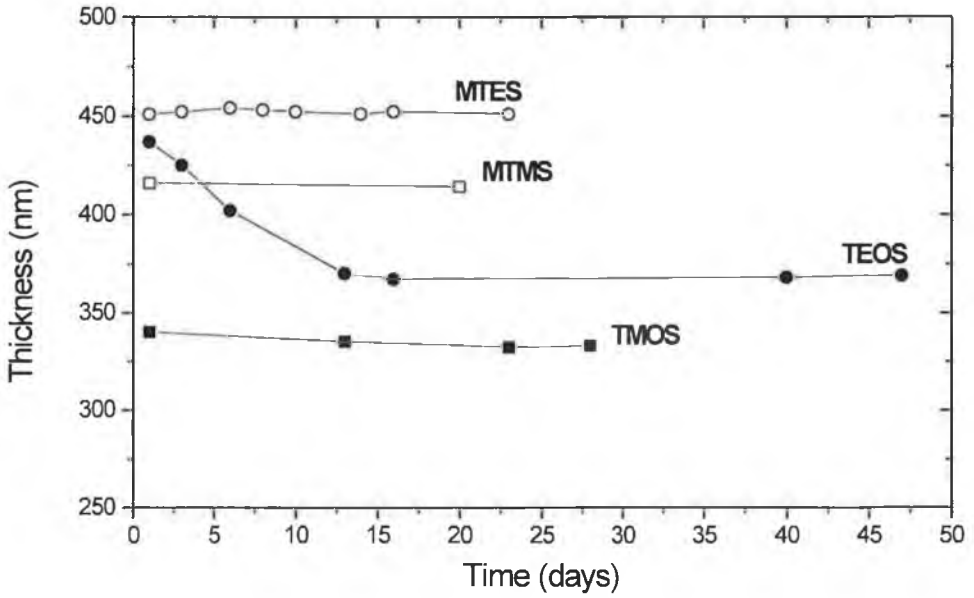

Figure 5.5 Temporal Behaviour of Doped R=2 pH=1 Films

5.6 Effect of Ultrasound on Film Thickness

As explained in section 4.2.2.4, using ultrasound on a sol can enhance the hydrolysis and condensation reactions and hence alter film properties. For this study, initially sols were sealed, placed in the ultrasound bath for 15 minutes and dipped immediately after sonication. The initial work for this study was carried out on MTES:TEOS 1:1 undoped films as the thickness stabilisation time is short and film quality is good. A study of time after sonication and before dip coating was carried out to try to optimise this method. The first studies were carried out by dip coating silicon substrates 5, 15, 30, 45, 60 and 75 minutes after sonication. It was found that thickness differences between 5 and 15 minutes were over 100nm. This effect is taken to be a consequence of pressure build up in the sealed vial during sonication due to evolution of ethanol

during the reactions. By piercing the lid of the vial during sonication this effect is not as dramatic and thickness differences are within 20nm.

Since ultrasound is reported to change the properties of the sol, for example the microstructure, a study was carried out to see if ultrasound has an effect on thickness stabilisation. For this TEOS films were fabricated doped and undoped, sonicated and stirred.

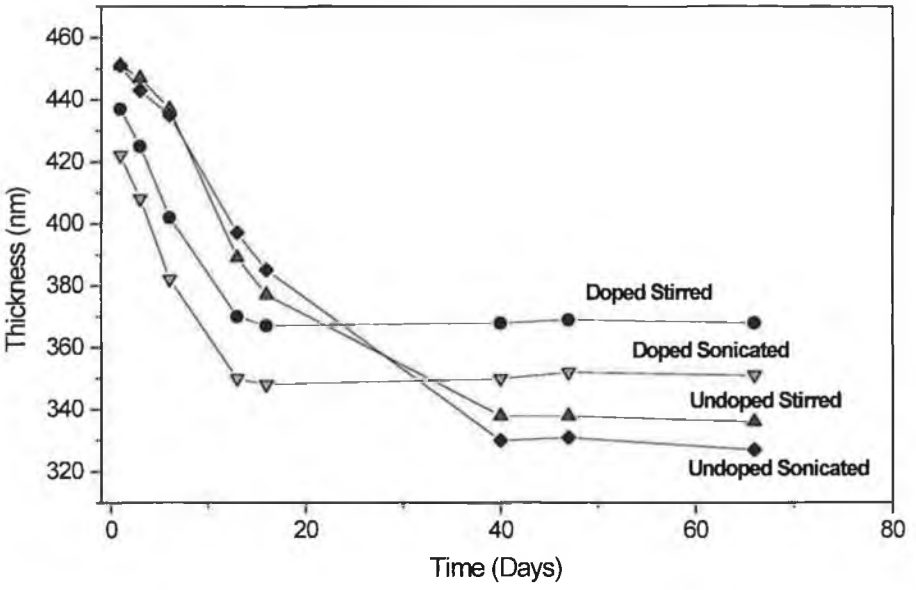

Figure 5.6 Effect of Ultrasound on Thickness

Figure 5.6 shows the results of this study. Clearly using ultrasound has no effect on stabilisation time and has no effect on film thickness (within the error). This is reflected in the oxygen quenching data in the next chapter. It is concluded that the ultrasonic bath has not enough power to alter the microstructure of the films and so the only effect of the ultrasound was mixing the sol more thoroughly but produces no obvious difference in film properties. In order to achieve an effect from ultrasound it

would be necessary to use an ultrasonic probe to produce more power[5]. The ultrasonic bath was calculated to be giving only 2.5 Wcm^{-2} whereas a probe would give over $400Wcm^{-2}$.

5.7 Summary

The rates of hydrolysis and condensation have an effect on film thickness. This has been illustrated by the differences in film thickness and thickness stabilisation times for TEOS films and MTES films. The effect of these rates can also be seen by changing precursor to TMOS and looking at its related precursor MTMS. The effect of introduction of a dopant into the sol-gel matrix enhances the hydrolysis rates. The mechanism for this is not yet known. In the following chapters these effects are reflected in the quenching data for the films.

5.8 References

[1] I.M. Thomas; **Optical Coating Fabrication**, *Sol-Gel Optics: Processing and Applications*, Kluwer Academic Publishers, Ed L. C. Klein, 1994, pp. 141-158

[2] C.M. McDonagh, F. Sheridan, T. Butler and B.D. MacCraith; **Characterisation of Sol-Gel Derived Silica Films**, *J. Non-Cry Solids*, Vol. 194, 1996, pp.72-77.

[3] F. Sheridan; **Characterisation and Optimisation of Sol-Gel Derived Thin Films for use in Optical Sensing**, MSc. Thesis, 1995, Dublin City University.(unpublished)

[4] C.J. Brinker, G.W. Scherer; **Sol-Gel Science: The Physics and Chemistry of Sol-Gel Processing**, Academic Press, San Diego, 1990, pp. 787.

[5] L. Esquivias, J. Zarzycki; **Sonogels: An alternative Method in Sol-Gel Processing**, in J.D. Mackenzie and D.R. Ulrich, Eds., *Ultrastructure Processing of Advanced Ceramics*, Proc. Conf., Feb 23-27, 1987, San Diego, C.A., pp 255-270, Wiley, N.Y., 1988

Chapter 6

Film Hydrophobicity

6.1 Introduction

This chapter looks at the hydrophobic properties of a range of sol-gel films. The first section explains why hydrophobicity is such an important parameter for the optical sensors programme. The results of contact angle measurements and FTIR spectral analysis are discussed.

6.2 Film Surface Properties

The reactions for hydrolysis and condensation are discussed in section 2.3. When TEOS is hydrolysed, Si-OH bonds are formed. If these groups do not react by condensation reactions they are termed terminal silanol groups. On the surface of a film fabricated from TEOS there are many of these silanol groups which make the TEOS film surface very hydrophilic since water can become hydrogen bonded to the surface. Figure 6.1 illustrates this phenomenon [1].

Organically modified precursors such as MTES generally have at least one Si-C bond. These bonds are non-hydrolysable and so the surface of an MTES film is made up predominately of $Si-CH_3$ groups. With TEOS films the Si-OH groups attract water but

the Si-CH_3 groups on the MTES surface repel water because of the hydrophobic nature of these groups.

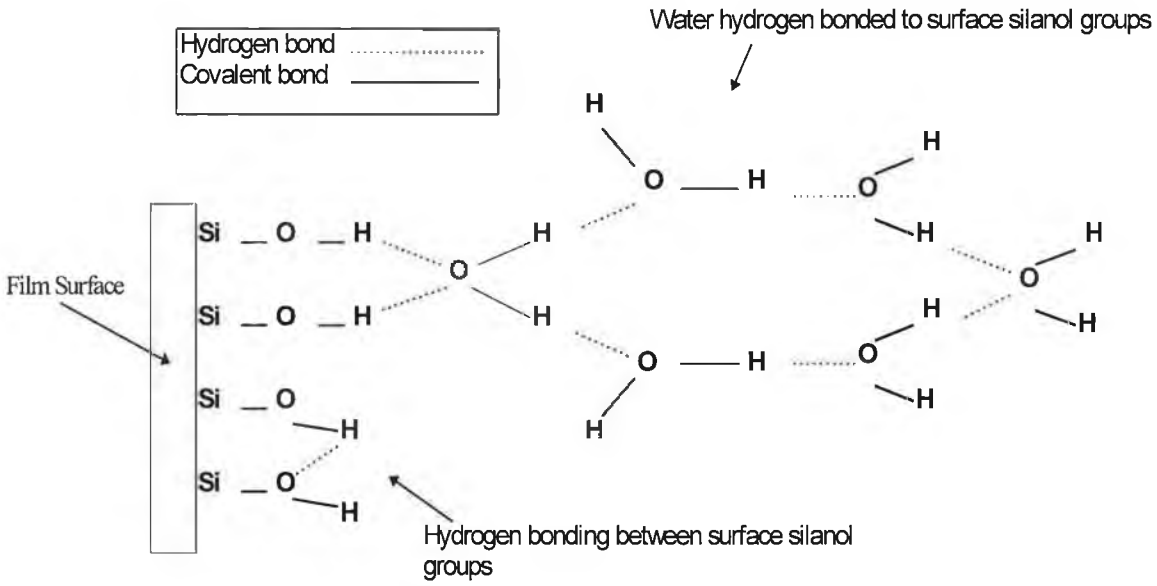

Figure 6.1 Water Hydrogen Bonded to the Surface of a TEOS Film.

Hydrophobicity of sol-gel films is crucial when using the films for dissolved oxygen sensing. This is due to the mechanism in which the dissolved oxygen travels to the entrapped ruthenium complex in order to quench its fluorescence. The oxygen partitions out of solution in order to access the ruthenium complex in the pores. Hydrophobic films such as those fabricated from MTES facilitate this by repelling the water but with hydrophilic films like TEOS it is more difficult for the oxygen to pass through the hydrogen bonded water on the surface of the film. This is reflected in the fluorescence quenching results in the next chapter.

6.3 Contact Angle Measurements

As discussed in section 4.4.2, dynamic contact angle measurements can be used to characterise film hydrophobicity. For this experiment films were fabricated from TEOS, TMOS, MTES and MTMS and their contact angles compared. The hysteresis loops for the four samples are shown in figures 6.2 (TEOS), 6.3 (TMOS), 6.4 (MTES) and 6.5 (MTMS). The most notable feature on the graphs is the difference in the position of the hysteresis loop along the force axis. The hysteresis loops for TMOS and TEOS are at a force well below zero whereas the hysteresis loops for MTES and MTMS are positioned much higher up the force axis. This is the first indication of the hydrophilic nature of TEOS and TMOS films.

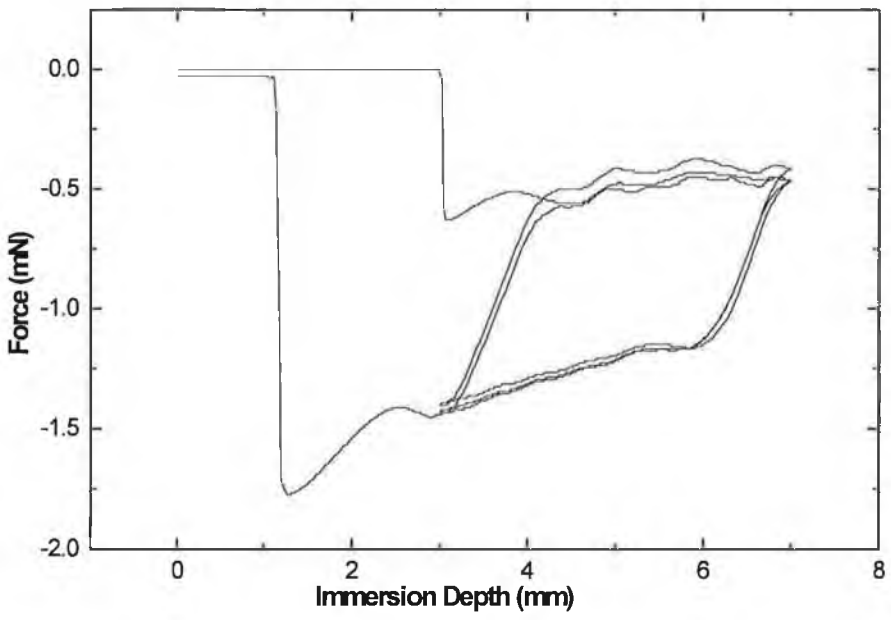

Figure 6.2 Typical Hysteresis Loop for TEOS Films

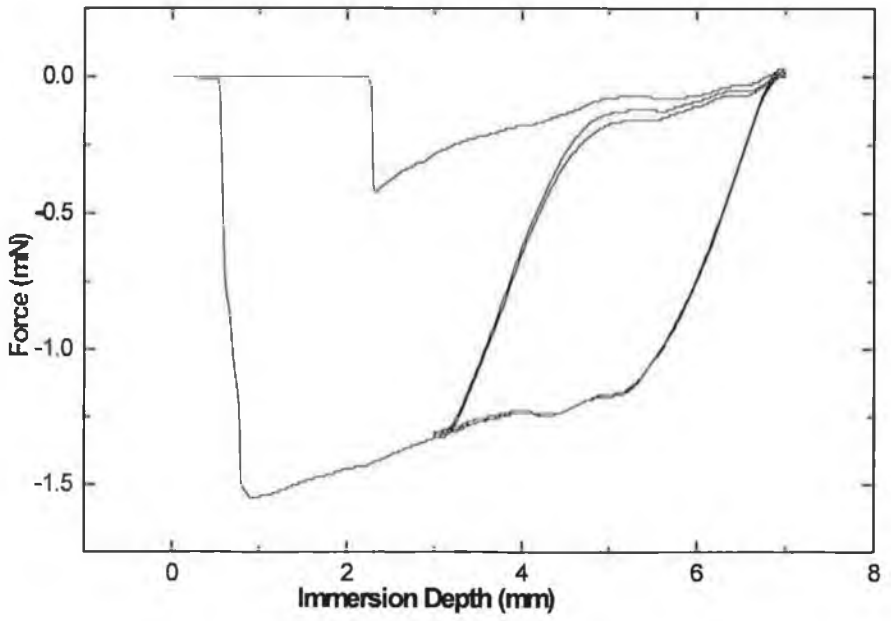

Figure 6.3 Typical Hysteresis Loop for TMOS Films

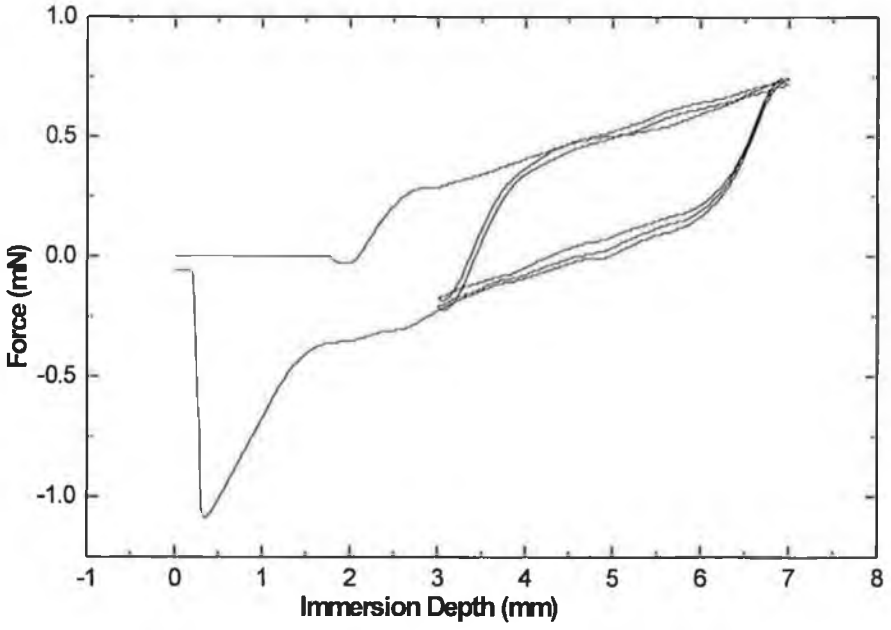

Figure 6.4 Typical Hysteresis Loop for MTES Films

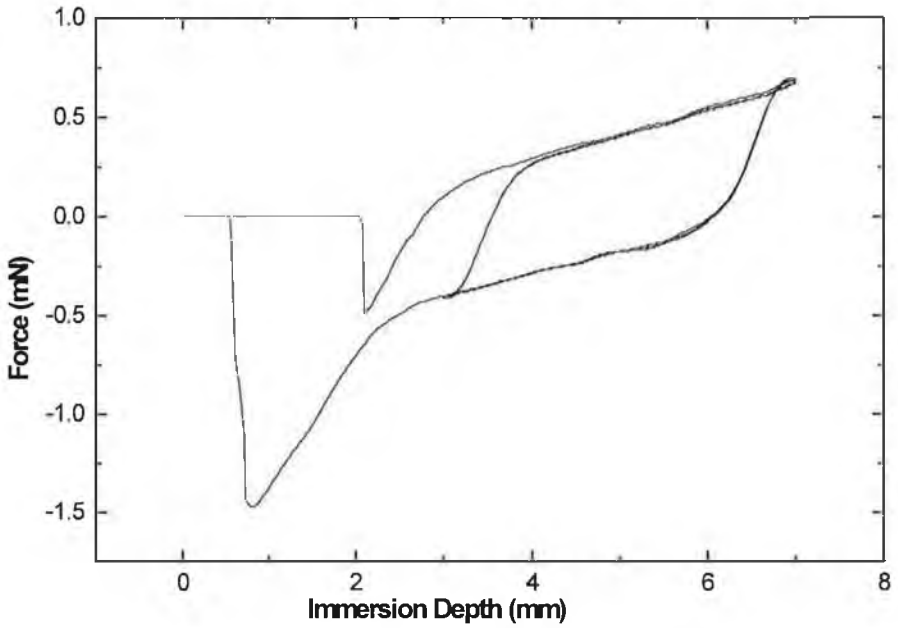

Figure 6.5 Typical Hysteresis Loop for MTMS Films

The advancing and receding forces (see figure 4.4) for all films are different due to the hysteresis loops and so the advancing and receding angles will differ from each other. The accepted way of interpreting these results is to use the equilibrium contact angle (θ_{eqm}) which is the average of the advancing and receding angles. Table 6.1 shows the equilibrium contact angle for the films.

TEOS and TMOS are hydrophilic and have small contact angles. These equilibrium contact angles indicate the relative hydrophobicity of the films. Since the apparatus is home-made and is being improved on an on-going basis, a good reference hydrophilic film (i.e. $Q_{eqm}=0$) has not been identified. In this work it is clear from other measurements that TMOS films are most hydrophilic while MTES and MTMS are most hydrophobic and the contact angle data are consistent with this.

	Contact Angle θ_{eqm} (+/- 3°)
TEOS	47°
MTES	80°
TMOS	40°
MTMS	82°

Table 6.1 Equilibrium Contact Angle Results

6.3.1 Qualitative Contact Angle Measurements

When a sample is cooled atmospheric moisture condenses onto the film surface. By looking at the shape of the droplets of water formed on the surface, the hydrophobicity of a sample can be qualitatively assessed.

For this experiment samples were placed on a peltier cooled platform whose temperature changed from 20°C to 4°C in one minute. As the samples cooled the formation of water droplets on the surface was observed using a Nikon microscope (model 272285) with an objective lens (20x10x100). Photographs were taken 1, 2 and 3 minutes after the sample was placed on the platform. The photographs taken at 3 minutes are shown in figures 6.6, 6.7, 6.8, 6.9, 6.10 and 6.11.

Spherical droplets are characteristic of hydrophobic films. From figures 6.6 and 6.9 it can be seen that the droplets formed on the TEOS film are slightly more spherical than the droplets formed on the TMOS film indicating that TMOS is more hydrophilic. This

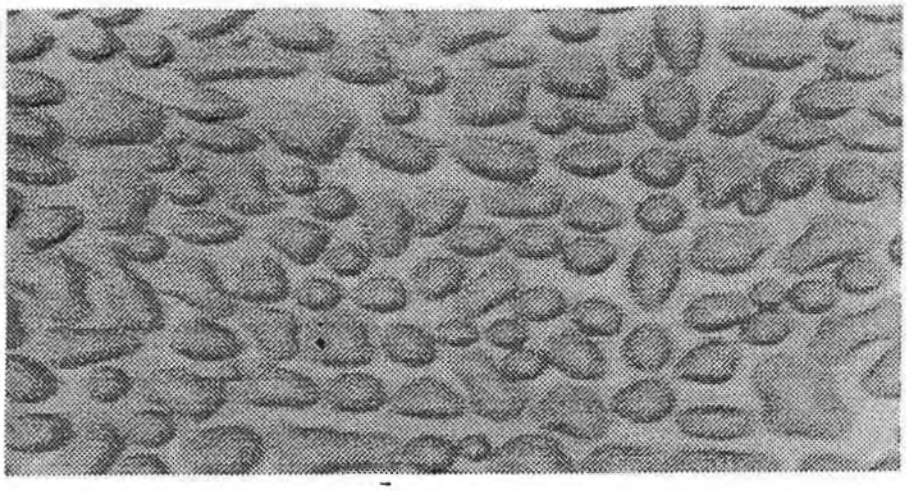

Figure 6.6 TMOS

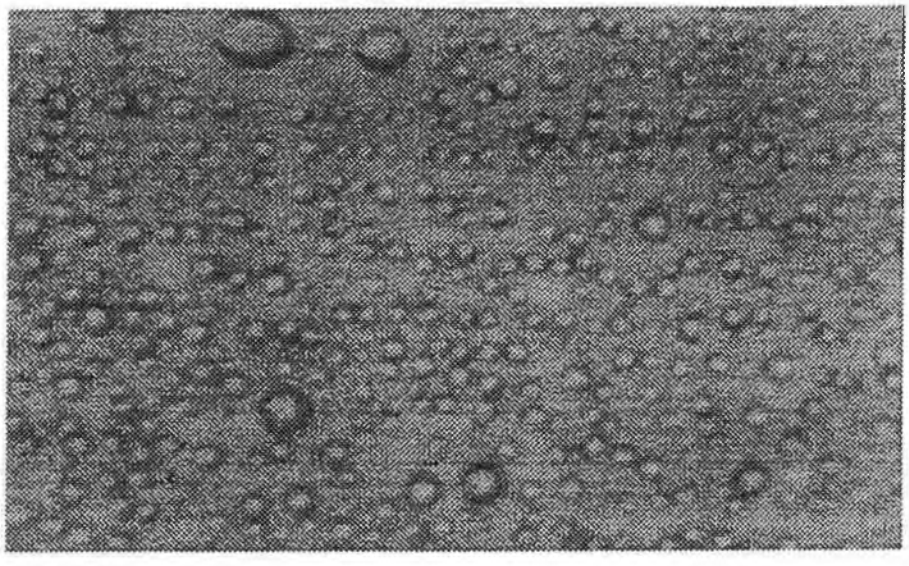

Figure 6.7 MTMS

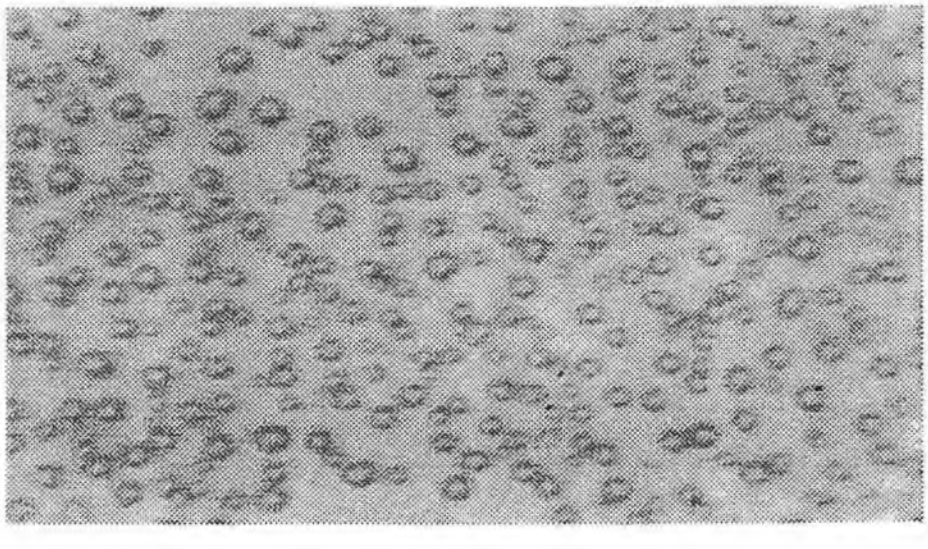

Figure 6.8 ETMS

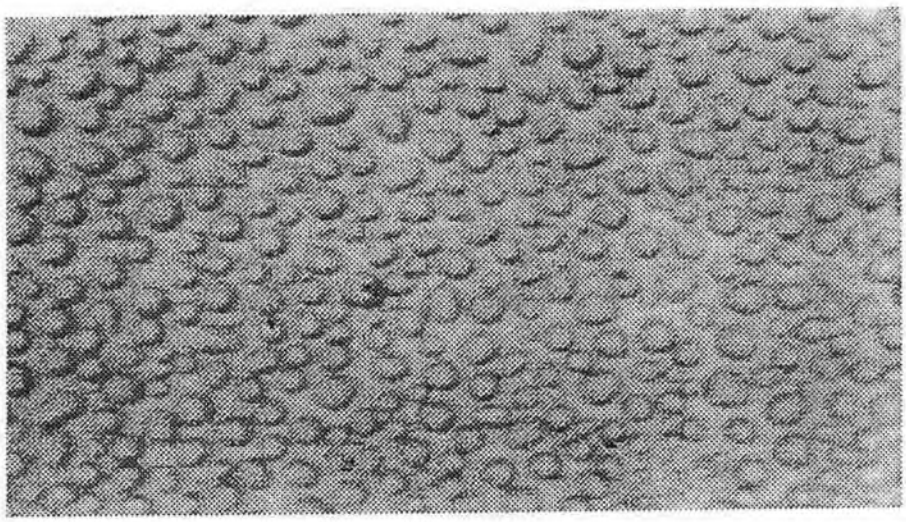

Figure 6.9 TEOS

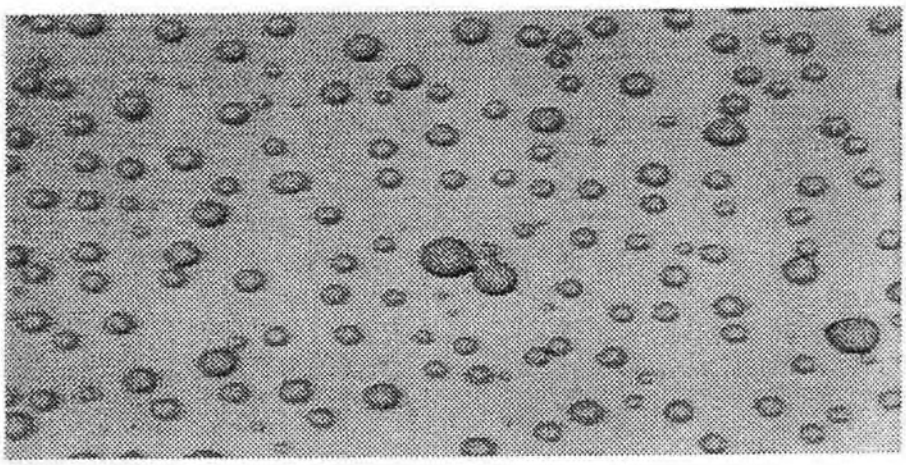

Figure 6.10 MTES

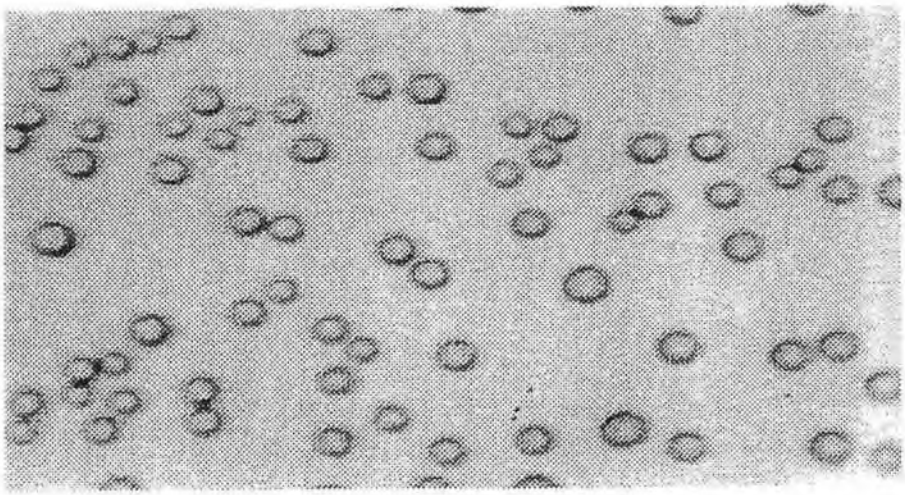

Figure 6.11 ETES

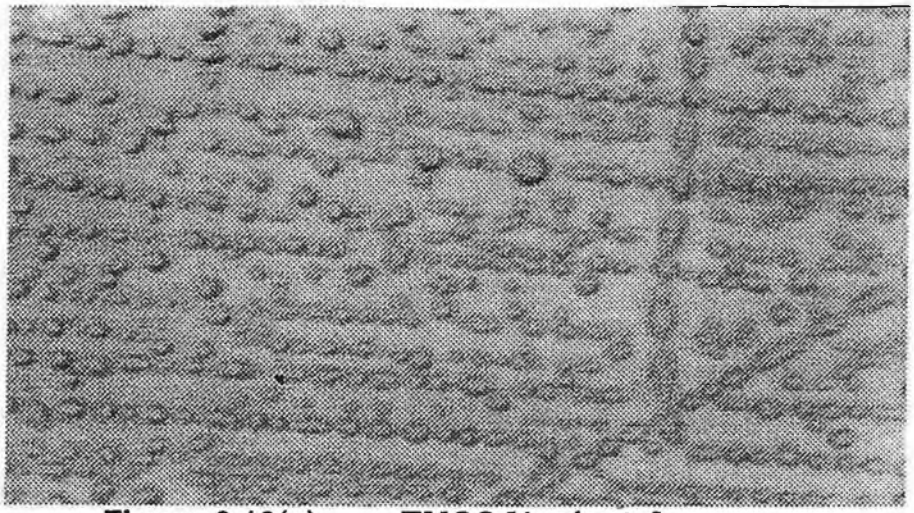

Figure 6.12(a) TMOS [1 minute]

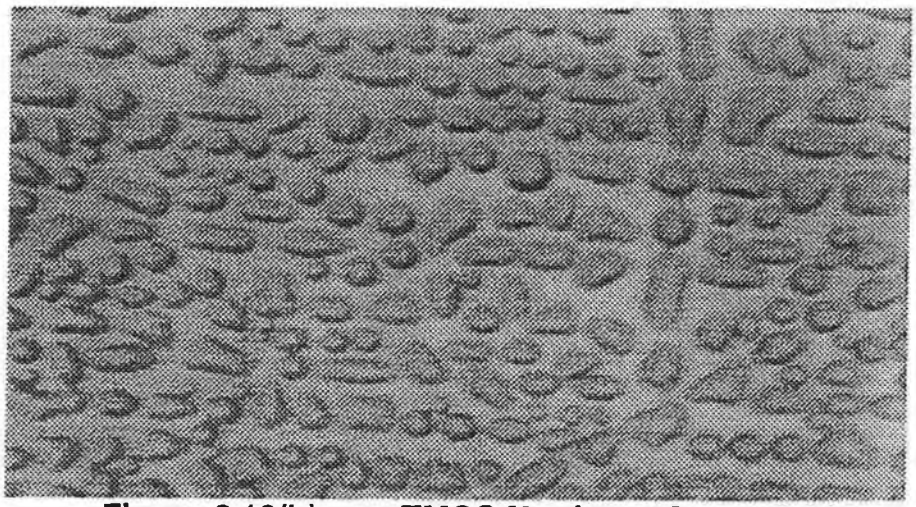

Figure 6.12(b) TMOS [2 minutes]

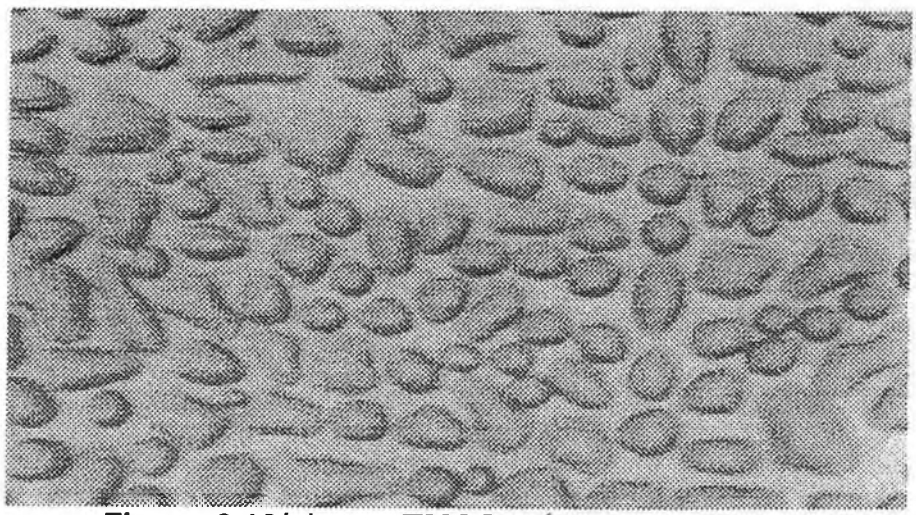

Figure 6.12(c) TMOS [3 minutes]

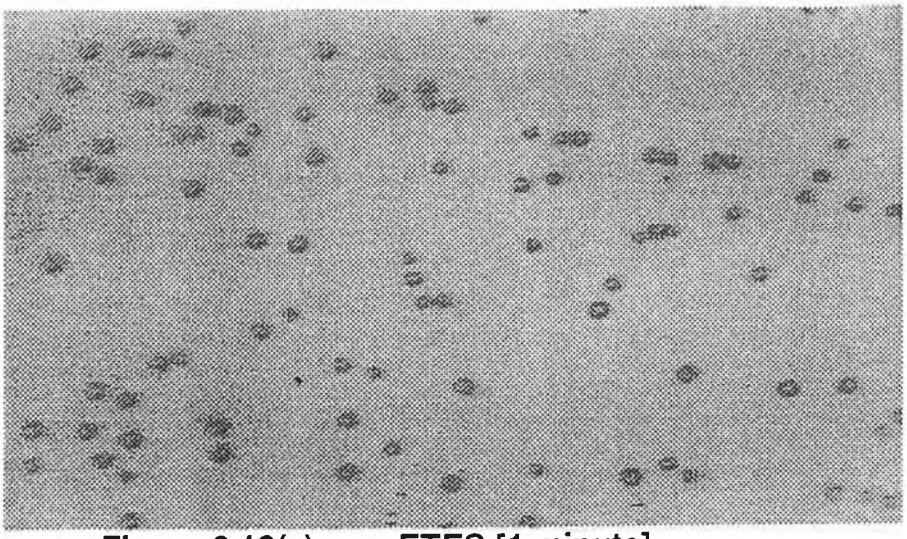

Figure 6.13(a) ETES [1 minute]

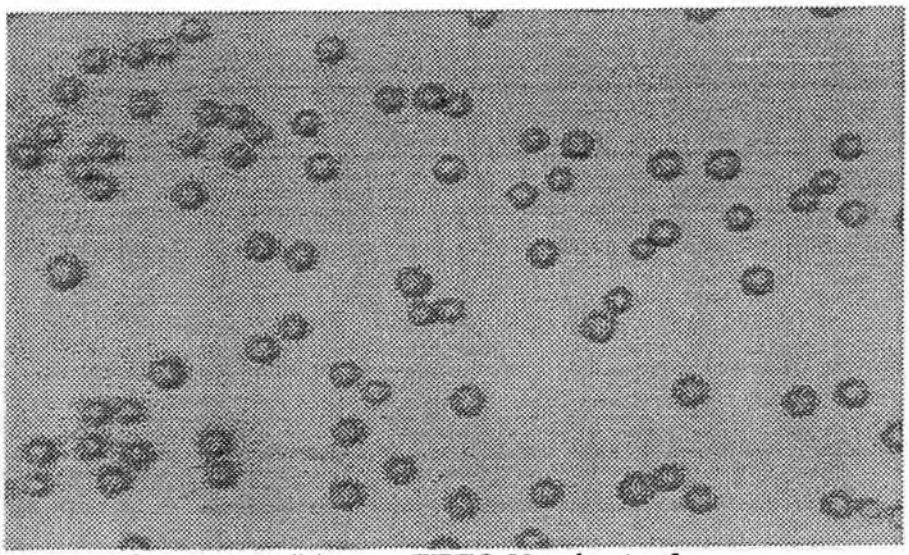

Figure 6.13(b) ETES [2 minutes]

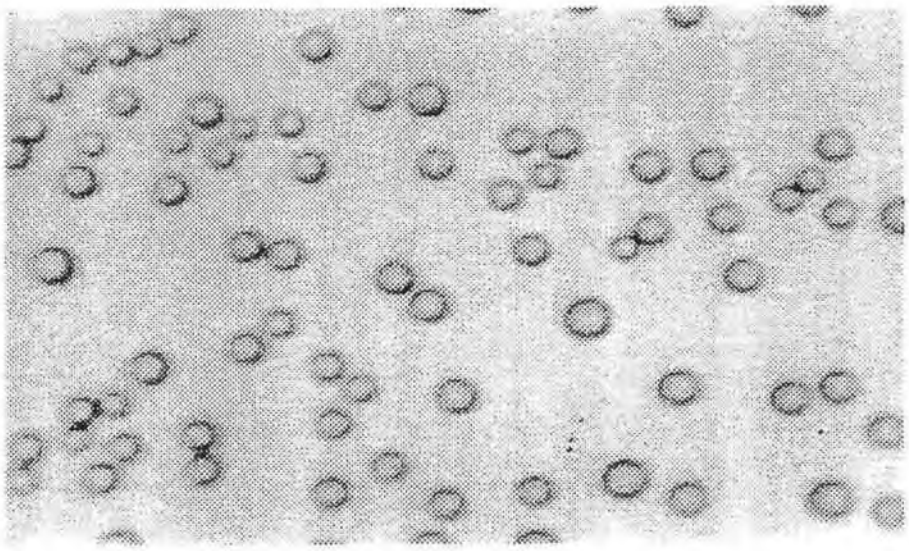

Figure 6.13(c) ETES [3 minutes]

agrees with the contact angle measurements shown in table 6.1. Films fabricated from organically modified precursors have spherical droplets characteristic of hydrophobic surfaces.

Figures 6.12 and 6.13 show TMOS, the most hydrophilic film, and ETES, a more hydrophobic film at 1,2 and 3 minutes after being placed on the platform. It can be seen that droplets form quickly on the surface of the TMOS film The droplets increase in size and join together wetting practically all of the film surface. For the film fabricated from ETES, the droplets form more slowly, are more isolated and do not wet the sample as much. It is clear that this qualitative but elegant study of relative hydrophobicity agrees with the more quantitative contact angle data.

6.4 FTIR Spectra

6.4.1 Hydrophobicity Investigation

The hydrophobicity of sol-gel films can also be investigated using FTIR spectral analysis. Hydroxyl groups adsorb in a broad infrared band at around 3400cm^{-1}. This is due to -OH stretching with contributions from hydrogen bonded internal silanols (3640cm^{-1}) and free surface silanols (3740cm^{-1}) [2]. The intensity of this band gives an indication of the hydrophobicity of the sample.

For this experiment films were fabricated from TEOS, TMOS, MTES and MTMS at R=2 and using water of pH=1. The films were coated onto silicon wafers. The spectrum of an uncoated silicon slide was subtracted by running the absorption spectrum of an uncoated substrate and then a sample spectrum with a background in air. The spectrum of the uncoated slide was subtracted from the sample spectrum by

normalising the uncoated silicon spectrum and creating a new background using equation 6.1 and then subtracting this from the sample spectrum.

$$\text{new background} = \text{silicon spectra} \times \frac{10 \text{ points sample}}{10 \text{ points silicon}} \qquad \textbf{(6.1)}$$

where 10 points sample and 10 points uncoated silicon are 10 data points of the absorption corresponding to the same wavenumber for both. This is to allow for correction because the infrared light does not have the same interaction distance between the sample and the uncoated slide due to the thickness of the sol-gel film.

The resultant sample spectra can be seen in figure 6.14.

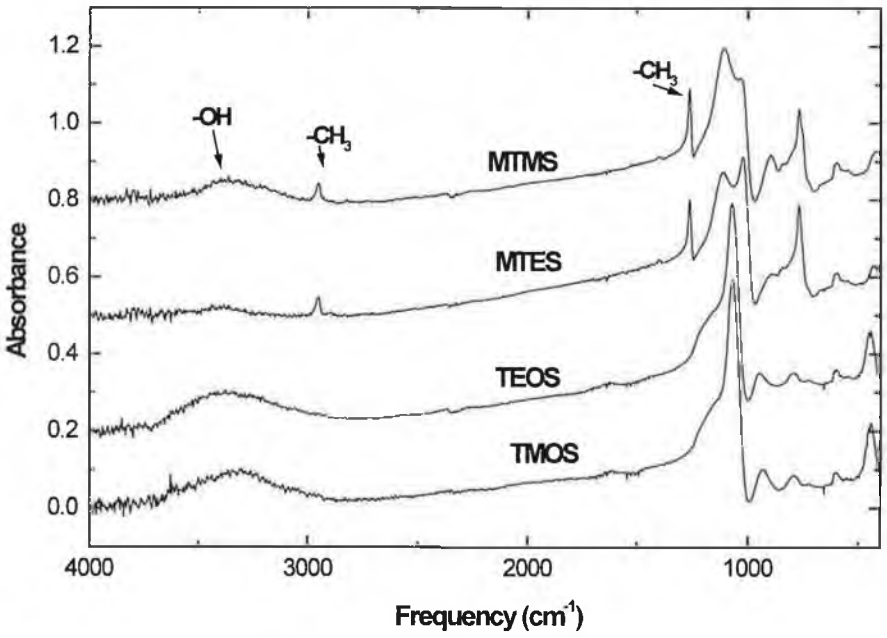

Figure 6.14 FTIR Spectra.

It can be seen that the band at 3400cm^{-1} is significantly reduced when comparing films fabricated from unmodified precursors i.e. TEOS and TMOS and films

fabricated from modified precursors MTES and MTMS. Molecular water absorbs in a weak band at around 1650cm^{-1} and it can be seen that this band is present on TMOS and TEOS spectra. This method of investigating the hydrophobicity proves to be a good method for distinguishing between films fabricated from unmodified and modified precursor. However the data presented here do not distinguish between TEOS and TMOS films. Generally the FTIR data agree with the contact angle results of the previous section.

6.4.2 Other Features

Other features on the spectra are ascribed according to Innocenzi *et al* [2]. These include C-H stretching at 1260cm^{-1} and 2900-3000cm^{-1} present on MTES and MTMS only, which are due to the methyl groups. These features are characteristic of ormosil films and are not present on TMOS and TEOS spectra. The dominant peak characteristic of the Si-O-Si bond is ascribed to a main high intensity peak at around 1070cm^{-1}. This band moves to lower wavenumbers for organically modified samples. This band is accompanied by a shoulder, which for TEOS and TMOS this is centred at around 1200cm^{-1}. It has been suggested [3,4] that the intensity of this shoulder can be correlated with the porosity of the sol-gel film and is activated by the sol-gel pores scattering the normally incident infrared light. If this theory is applied to the spectra shown in figure 6.14, then TEOS and TMOS have approximately the same porosity whereas MTES and MTMS are less porous. This is expected as reduced porosity is in agreement with a higher condensation rates and the greater flexibility of the modified network [3].

6.5 Summary

Hydrophobicity of sensor films is an important parameter when using the films for dissolved oxygen sensing because of the mechanism by which the oxygen travels to the entrapped ruthenium complex in the pores. Larger contact angles for films derived from organically modified precursors indicate greater hydrophobicity than either TEOS or TMOS. This is consistent with reduced -OH band intensity at ~3400cm^{-1} for MTES and MTMS films. The hydrophobic nature of MTES and MTMS films is correlated with sharp -CH_3 bands at 1260cm^{-1} and 2900cm^{-1} (-CH_3 replaces -OH).

6.6 References

[1] C.J. Brinker, G.W. Scherer; Sol-Gel Science: **The Physics and Chemistry of Sol-Gel Processing**, Academic Press, San Diego, 1990.

[2] P. Innocenzi, M.O. Abdirashid, M. Gugleilmi; **Structure and Properties of Sol-Gel Coatings from Methlytriethoxysilane and Tetraethoxysilane**, *J. Sol-Gel Sci. Technol.*, 1994, Vol.3, pp. 47-55.

[3] R.M. Almeida, G.C. Pantano; **Structural Investigation of Silica Gel Films by Infrared Spectroscopy**. *J. Appl. Physics*, Vol. 68, pp 4225, 1990.

[4] R.M. Almeida, H.C. Vasconcelos; **Relationship Between Infrared Absorption and Porosity in Silica Based Sol-Gel Films**, *Proc. SPIE* , 1994, Vol. 2288, pp. 678-687.

Chapter 7

Fluorescence Quenching Results

7.1 Introduction

The aim of this project is to develop and characterise sol-gel derived thin films for use in optical sensor applications. In order to achieve this the system shown in figure 4.5 was used to investigate the sensor response of various sol-gel films. This chapter details the method for characterising sensor response and the fluorescence quenching results are given for a range of thin films. The fluorescence lifetime of the entrapped ruthenium complex was investigated for different sol-gel films and the results are shown.

7.2 Fluorescence Quenching

The fluorescence quenching of the oxygen sensitive ruthenium complex was investigated for gas phase (dry) oxygen, 100% humidified gas phase oxygen and dissolved oxygen. The experimental methods are described in chapter 4.

In order to compare the quenching response of the sensor films fabricated from different precursors, the quenching response is given by the parameter Q defined as follows:

$$Q_{\text{Gas Phase}} = Q_{GP} = \frac{I_{N_2} - I_{O_2}}{I_{N_2}} \qquad (7.1)$$

where I_{N_2} is the fluorescence intensity measured in 100% nitrogen gas i.e. ~0% oxygen and I_{O_2} is the fluorescence intensity measured in 100% oxygen.

$$Q_{\text{Humidified Gas Phase}} = Q_{HG} = \frac{I_{N_2} - I_{O_2}}{I_{N_2}} \qquad (7.2)$$

Where I_{N_2} is measured in 100% humidified nitrogen and I_{O_2} is measured in 100% humidified oxygen.

$$Q_{\text{Dissolved Oxygen}} = Q_{DO} = \frac{I_{deoxy} - I_{oxy}}{I_{deoxy}} \qquad (6.3)$$

where I_{deoxy} is measured in deionised water that has had nitrogen bubbled through it so that it is *deoxygenated* water (it is very difficult to remove all oxygen from the water) and I_{oxy} is measured in deionised water that has had oxygen bubbled through it so that it is *oxygenated* water.

A typical quenching response for gas phase quenching of the ruthenium complex entrapped in ETMS is shown in figure 7.1 and the response for dissolved oxygen (DO) in figure 7.2. The most obvious difference in these responses is the slower response time of the DO for the same film. This is due to the slower diffusion coefficient of oxygen in aqueous phase. The relative size of the quenching coefficient Q also changes with quenching environment. This will be discussed in the following sections.

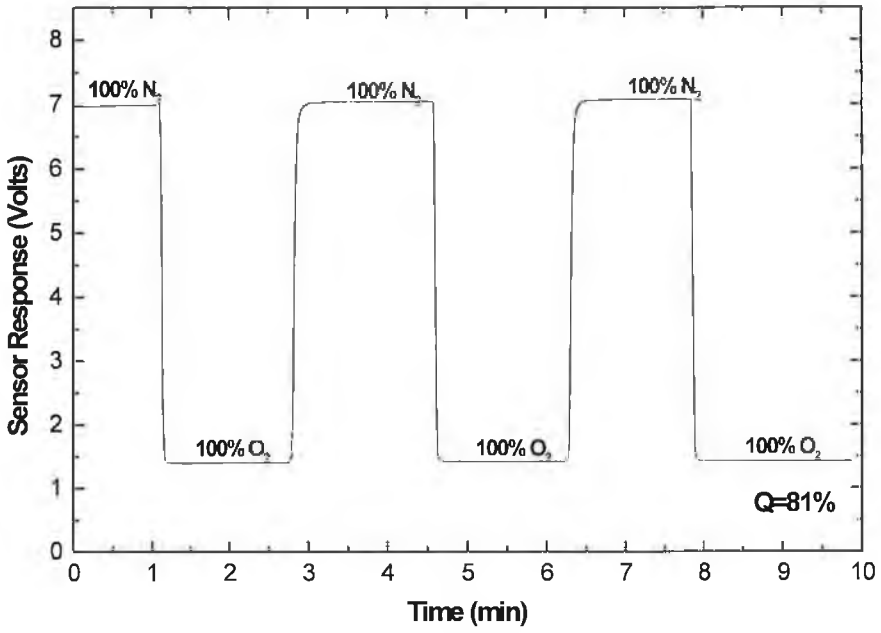

Figure 7.1 Gas Phase Oxygen Quenching Response for an ETMS Film

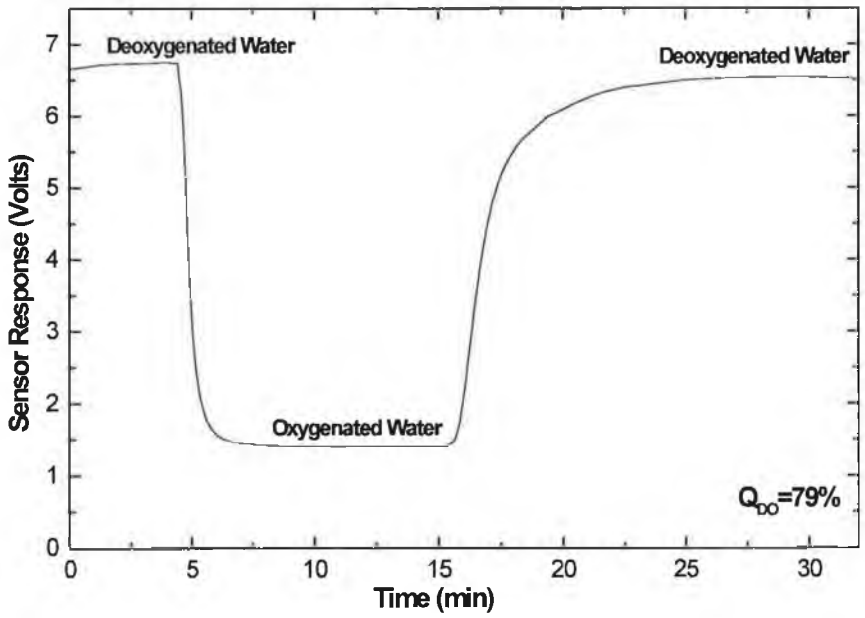

Figure 7.2 Dissolved Oxygen Quenching Response for an ETMS Film

7.3 TEOS and Related Ormosil Films

For this study films were fabricated from TEOS, MTES and ratios of TEOS:MTES 1:1, 2:1 and 3:1. Their quenching response was studied in gas phase oxygen, 100% humidified gas phase oxygen and in dissolved oxygen. The results are shown in table 7.1.

	Q_{GP} ± 2%	Q_{HG} ± 2%	Q_{DO} ± 2%
TEOS	94%	34%	30%
MTES:TEOS 1:1	97%	62%	52%
MTES:TEOS 2:1	93%	67%	59%
MTES:TEOS 3:1	84%	69%	62%
MTES	82%	75%	69%

Table 7.1 Quenching Results for TEOS and Related Ormosils.

TEOS films have a very good quenching response in gas phase oxygen. However the dissolved oxygen quenching for these films is very low due to the hydrophilic nature of the film thus reducing the ability of the oxygen to diffuse through to the entrapped oxygen as discussed in section 6.2. This makes the film very moisture sensitive which is reflected in the humidified gas phase response which is almost as low as the dissolved oxygen quenching response.

Due to the unhydrolysable Si-CH_3 bond in MTES, films fabricated with more of this precursor incorporated into the sol-gel matrix will be more hydrophobic hence less sensitive to moisture and resulting in a better quenching response in dissolved

oxygen. This is because the hydrophobic groups increase the partitioning effect discussed in section 6.2 and so more oxygen gas will come out of solution. It can be seen from table 7.1 that films with more MTES incorporated give better humidified gas phase results and better dissolved oxygen quenching.

The gas phase quenching decreases slightly with increasing MTES content, due to partial blocking of the pores by the CH_3 groups and so making it harder for the gas phase oxygen to access the dye.

7.3.1 Effect of Ultrasound

TEOS samples were made up at R=2 and using water of pH=1. The sols were treated with ultrasound in an ultrasonic bath for 15 minutes. The quenching measurements agreed with the thickness measurements, showing that there is no obvious difference in quenching response in gas phase oxygen or dissolved oxygen compared to samples fabricated from sols that had been stirred.

7.3.2 Effect of pH

Section 2.3.1 details the effect of pH on hydrolysis and condensation reactions. To investigate the effect that this has on the quenching response of the films MTES films were fabricated at R=2 and using water of pH= 1, 2.5 and 4.

MTES pH=1 sols do not require ageing and give good quality coating immediately after stirring. MTES pH=2.5 sols require ageing for 18 hours at room temperature in order to give good quality films. These films are not as thick as pH=1 films which indicates slower hydrolysis and condensation reactions, however this should have no effect on the quenching results[1]. MTES pH=4 sols require ageing for 18 hours at 70°C in order to coat the substrate. These films are of bad quality and the sol did not

gel one year after synthesis, indicating very slow condensation rates. The quenching results for these films are shown in table 7.2

MTES	Q_{GP} ± 2%	Q_{HG} ±2%	Q_{DO} ±2%
pH=1	82%	75%	69%
pH=2.5	82%	78%	74%
pH=4	86%	82%	73%

Table 7.2 Quenching Results for MTES Films Fabricated using Water at Different pH Values.

There is no significant difference in the gas phase quenching response for all films. The slight increase in the gas phase and humidified gas phase quenching response for pH=4 films appears to indicate a larger pore size with higher pH which is consistent with known hydrolysis and condensation behaviour at this pH[2]. However the dissolved oxygen quenching for the films does not exhibit the same trend. This is thought to be because dissolved oxygen quenching is dependent on the partitioning effect facilitated by the hydrophobicity of the film rather than on the pore size[3]. It is concluded that acid-catalysed pH=1 films are the optimum for both gas phase and DO quenching. This is discussed further in section 7.4.3 on leaching effects.

7.4 TMOS and Related Ormosil Films

The first part of this study involved fabricating films from TMOS, MTMS and MTMS:TMOS 1:1 at R=2 and using water of pH=1. The gas phase and dissolved oxygen quenching results can be seen in table 7.3

	Q_{GP} ± 2%	Q_{DO} ± 2%
TMOS	71%	0%
TMOS:MTMS 1:1	73%	17%
MTMS	78%	60%

Table 7.3 Quenching Results for TMOS and Related Ormosil Films

TMOS films exhibit reduced quenching for gas phase oxygen and show no dissolved oxygen quenching. The dissolved oxygen quenching for MTMS:TMOS 1:1 is significantly reduced compared to MTMS. The lack of DO quenching for TMOS is thought to be due to the more hydrophilic nature of the film whereby oxygen partitioning does not occur. In the gas phase, the reduced quenching may be partially due to smaller pore size due to faster hydrolysis and condensation rates compared to TEOS. This is corroborated by leaching results in section 7.4.3. The hydrogen bonded water on the pore surface may also reduce gas phase oxygen diffusion through the network. The TMOS:MTMS mixed films exhibit intermediate behaviour while the MTMS films show gas phase and DO quenching slightly lower than for MTES again

due to lower diffusion coefficients as a result of increased density. This is discussed further in section 7.4.2.

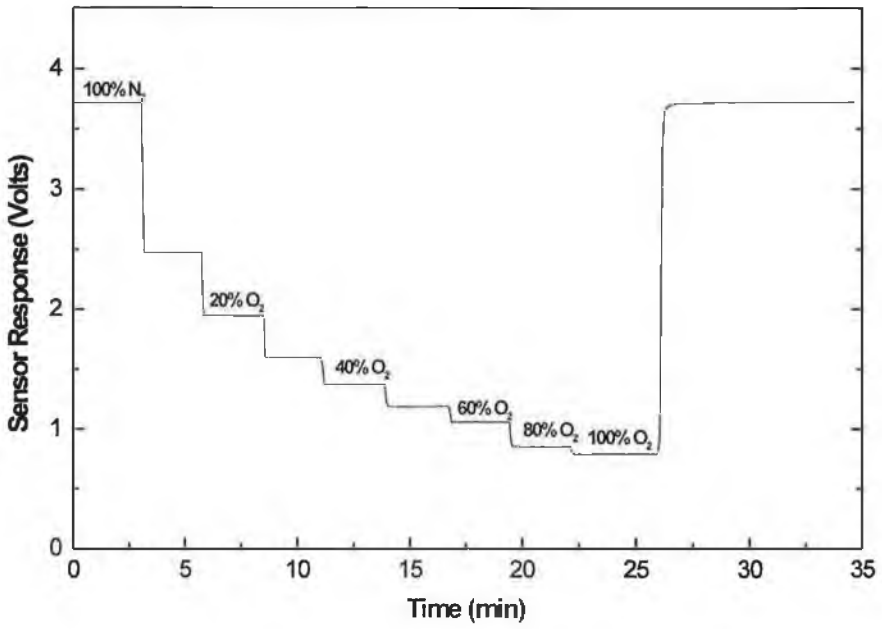

Figure 7.3 Typical Gas Phase Quenching Response for MTMS R=2 Film

7.4.1 Stern Volmer Plots

The gas phase quenching response of TMOS and MTMS films was investigated at different concentrations of oxygen. A typical quenching response graph is shown in figure 7.3. The main factor governing gas phase sensor response is the oxygen diffusion coefficient in the sol-gel film. This is governed by the stern Volmer equation (eqn. 3.2) which predicts a non-linear decrease in fluorescence intensity as a function of oxygen concentration. Figure 7.3 shows the biggest drop in intensity at low oxygen

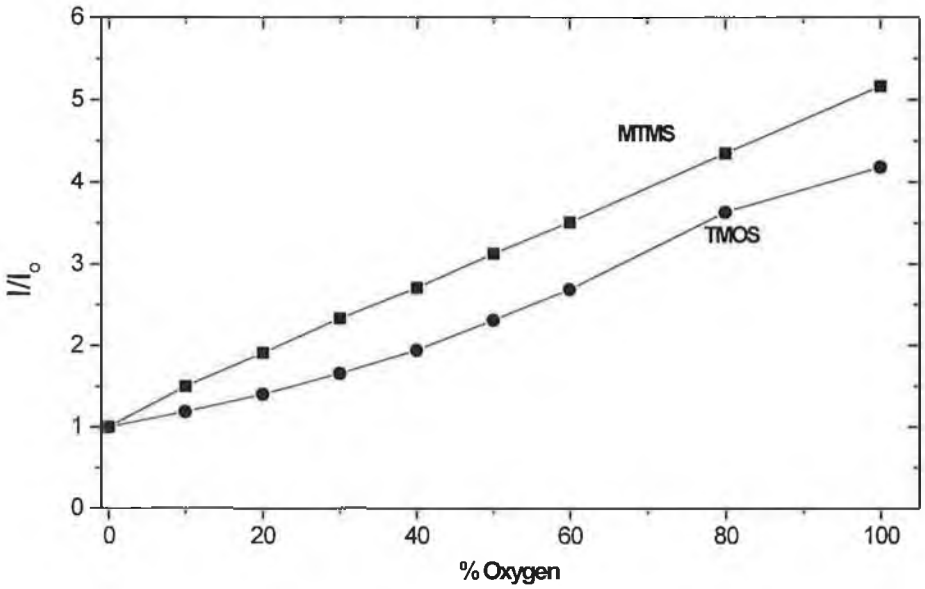

Figure 7.4 Stern-Volmer Plots for MTMS and TMOS R=2 Films

concentration i.e. 0% $O_2 \rightarrow 10\%O_2$ and there is a very small drop between 80 and 100% oxygen as predicted.

A Stern-Volmer plot of I_o/I against quencher concentration should theoretically give a straight line of slope K_{SV} and an intercept of 1 on the Y-axis. From figure 7.4 it can be seen that this is true of MTMS. However TMOS gives a curved response. This deviation from linearity is due to the inhomogenety of the fluorophore environment. TMOS sols have very fast hydrolysis and condensation rates which may lead to uneven distribution and clustering of the dye molecules.

7.4.2 Comparison with TEOS

This part of the study involved fabricating films from TMOS, MTMS and ETMS and comparing them to the corresponding TEOS and related ormosil films MTES and

ETES. Table 7.4 shows the results of this investigation for gas phase, humidified gas phase and dissolved oxygen.

	Q_{GP}	Q_{HG}	Q_{DO}
TEOS	96%	34%	30%
TMOS	71%	4%	0%
MTES	85%	75%	69%
MTMS	78%	65%	60%
ETES	87%	85%	82%
ETMS	82%	81%	79%

Table 7.4 Comparison Results

Overall quenching responses for films fabricated from TEOS and related organically modified precursors are higher than the corresponding values for films fabricated from TMOS and related organically modified precursors, for gas phase, humidified gas phase and dissolved oxygen quenching. The hydrolysis and condensation rates for TMOS are much faster than for TEOS due to less steric hindrance as discussed in chapter 2. As a result of this TMOS films are more dense i.e. less porous than TEOS films and so the quenching responses are reduced due to lower diffusion coeffiecents. The most pronounced difference between results for TEOS and TMOS films is that TMOS is the more hydrophilic as shown by the DO quenching results in table 7.4 and also by hydrophobicity measurements in chapter 6. By using organically modified precursors to produce hydrophobic films, the relative difference in quenching results

becomes less. For example there is very little difference in quenching results between ETES and ETMS films.

The main advantage of using organically modified precursors for gas phase sensing is demonstrated in the reduced sensitivity of the films to humidity by introducing a hydrophobic CH_3 or C_2H_5 group into the sol-gel matrix. It can be seen that for the most hydrophobic film the difference in quenching for the three environments is minimised. This can be seen most clearly by comparing TMOS, which has no dissolved oxygen quenching and very little quenching in humidified gas phase oxygen, to ETMS which within the error, has similar responses in all three environments. ETES films exhibit similar responses. The results of this investigation clearly show that the optimum sensor films for both gas phase and dissolved oxygen sensing are those fabricated from ETES or ETMS due to their high quenching response and humidity insensitivity. A major factor in the sensing of gases is the effect of humidity on sensor response and the results of this work indicate that ETES and ETMS ormosil films are excellent candidates for both gas-phase and DO oxygen sensing.

7.4.3 Leaching Studies

A common problem encountered with sol-gel sensor films is leaching. Leaching is the term used to describe the process whereby the entrapped dye complex comes out of the sol-gel matrix when the film is placed in a liquid for example water. In this laboratory it has been found that MTES R=2 films leach by about 12% over 60 hours this is reduced to 1% by altering the R value for example using films fabricated at R=4. Previous work in this laboratory has established that increased R-value for pH=1 films results in smaller average pore size, hence reduced leaching. For this study films

fabricated from TEOS, TMOS and MTMS are placed in the sensor cell and aerated deionised water is pumped through the cell in a closed system. The sensor response is recorded over 40 hours. All films used are well characterised i.e. they had been characterised for gas phase, humidified gas phase and dissolved oxygen. This is done so that the results obtained are less likely to be a result of photobleaching. Figure 7.5 shows the results of this study.

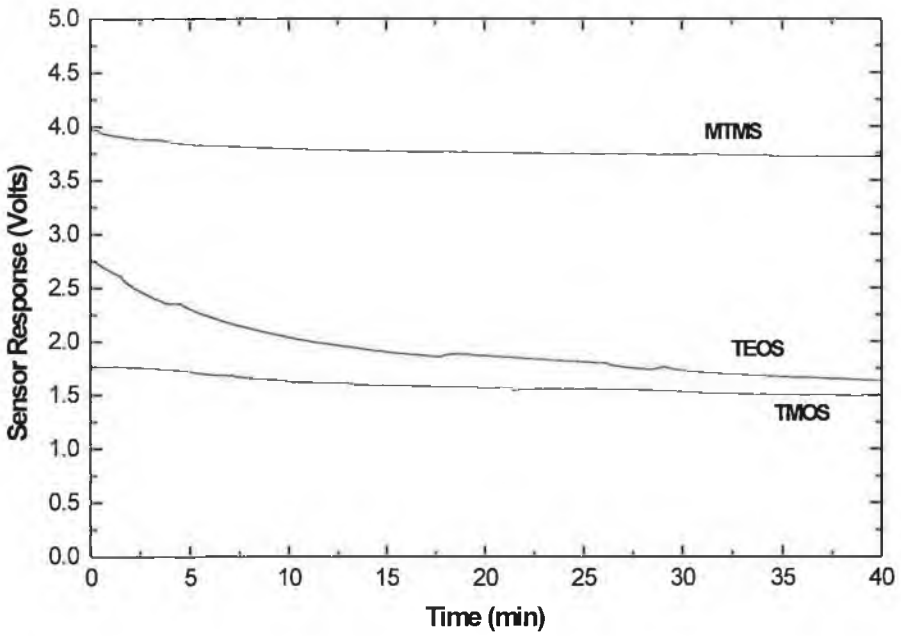

Figure 7.5 Leaching studies of TEOS, TMOS and MTMS

It can be seen from the graph that films fabricated from TEOS leach the most over the 40 hour time period, the intensity drops by 41% of the initial value. TMOS and MTMS films do not leach as much. The intensity of MTMS drops by only 6% and TMOS drops by 15%. This reduced leaching is an indication of the more dense structures of TMOS and MTMS films compared to TEOS due to faster hydrolysis and condensation rates. These results indicate that MTMS films will exhibit superior

performance for DO sensing compared to MTES fils as dye leaching for R=2 films is reduced by a factor of two compared to MTES films. As discussed at the beginning of this section, leaching can be almost eliminated by increasing the R-value in film fabrication. As discussed in section 7.3.2, film fabrication at higher than pH=1 has no advantage with regard to quenching. It has also been established in previous studies that film quality deteriorates with increasing pH and also dye leaching increased due to increased pore size.

7.5 Fluorescence Decay Time Analysis

Decay time based sensors have advantages over intensity based sensors as discussed in section 3.4. In order to investigate the viability of such a sensor studies were carried out on a range of samples. The system used for decay time analysis is shown in figure 4.7. For this study films were fabricated from TEOS, TMOS, MTES, MTMS, ETES and ETMS at R=2 and using water of pH=1. Investigations were carried out in air and in 100% nitrogen. A typical decay curve is shown in figure 7.5. For all samples curves were fitted to a single exponential and a double exponential decay in a graphing package called Origin. It was found that contrary to results found previously[3,4] all samples were more accurately fitted to a single exponential decay both in air and 100% nitrogen.

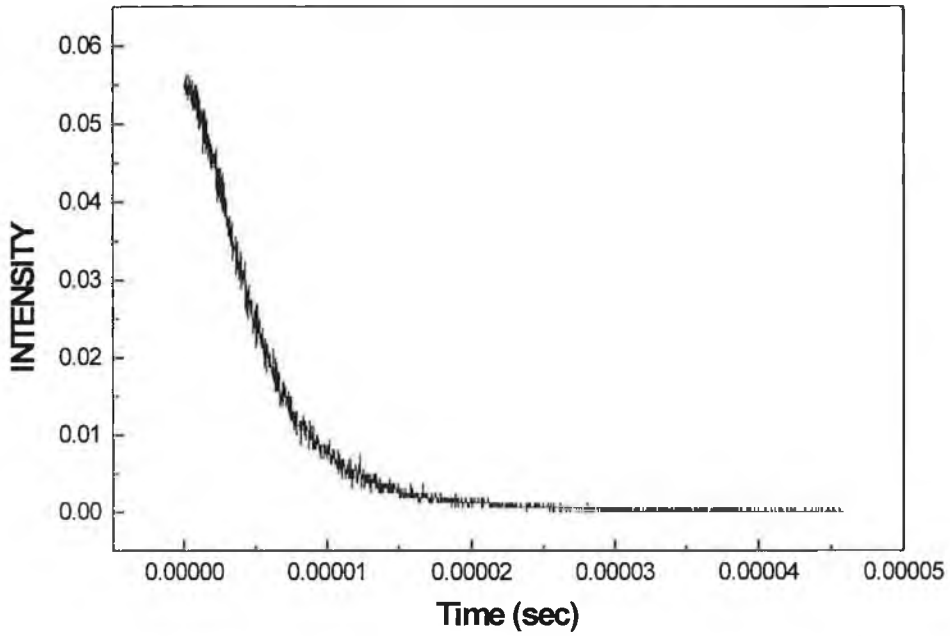

Figure 7.5 Typical Fluorescence Decay Curve

Another method of finding the decay time was also used which involved calculating the area under the decay curve using equation 4.4. The results for this study are shown in table 7.5

To show how big an error is associated with this method of determining fluorescence decay time two results are shown for each precursor. It can be seen from the table that this error is large and so the results are only quoted to one decimal place. It can also be seen that there is no obvious trend or difference between precursors. However there is a difference in decay time between ambient air and 100% nitrogen which is expected[3].

The decay time of the ruthenium complex does not change within the error when looking between sol-gel films fabricated from different precursors. One of the main reasons of using Ruthenium diphenlyphenanthroline is because it has been found to be less sensitive to the sol-gel environment that other oxygen sensitive dyes[5].

However it is expected that the decay time will differ slightly for films fabricated with different precursors. It is clear from the data presented here that this method of determining decay time is too inaccurate to be able to make any statements about the effect of the sol-gel matrix on decay time. It is thought that the pulse-to-pulse intensity variation in the Nd-YAG laser is the source of noise in the system which obscures any trend in decay time. Since characterisation of decay time is an important preliminary step in implementing phase-fluorimetric based sensors, it is proposed to build a pulsed LED system for decay time measurements.and so a more accurate method of measurement would be needed in order to quantify the effect of precursor on decay time.

	Ambient Air (μs)		Nitrogen (μs)	
	τ Average	τ 1st Exp.	τ Average	τ 1st Exp.
TEOS	5.4 5.2	5.3 5.1	6.0 5.9	5.9 5.6
MTES	5.2 5.6	5.1 5.7	6.4 7.6	6.4 8.4
ETES			5.7 5.3	5.5 5.3
TMOS	4.7 5.1	4.5 4.8	5.3 6.9	4.8 7.1
MTMS	5.5 5.6	5.5 5.9	7.6 6.9	8.4 7.6
ETMS			6.8 6.7	6.4 6.9
Ru in solution.	1.3 1.1	0.8 0.9		

Table 7.5 Fluorescence Decay Time Results.

7.6 Summary

The fluorescence quenching response was looked at for a range of films in gas phase, humidified gas phase and dissolved oxygen. The results show the correlation between hydrophobicity and quenching response. ETES and ETMS films are the optimum sensor films for both gas phase and dissolved oxygen.

Fluorescence decay time measurements were investigated, however the method used was too inaccurate to be able to correlate between sol-gel precursor and decay time.

7.7 References

[1] F. Sheridan; **Characterisation and Optimisation of Sol-Gel Derived Thin Films for use in Optical Sensing**, MSc. Thesis, 1995, Dublin City University (unpublished).

[2] A.K. McEvoy; **Development of an Optical Sol-Gel Based Dissolved Oxygen Sensor**, PhD. Thesis, 1996, Dublin City University (unpublished).

[3] M.T Murtagh, et al.; **Luminescence Decay Analysis of Doped Sol-Gel Films,** *Proc. Soc. Photo-Opt. Instrum. Eng.,*. Vol. 2836, pp 87-96, 1996.

[4]P.F. Kiernan; **Oxygen Sensitivity of Ruthenium- Doped Sol-Gel- Derived Silica Films**, M.Sc. Thesis, 1994, Dublin City University (unpublished).

[5] K.F. Mongey, J.G. Vos, B.D. MacCraith, C.M. McDonagh, C. Coates, J.J. McGarvey; **Photophysics of mixed ligand polypyridyl ruthenium (II) complexes immobilised in silica sol-gel monoliths**, *J. Mater. Chem.*, 1997, Vol. 7 No. 8 pp 1473-1479.

Chapter 8

Conclusion

8.1 Conclusion

This project looked at a range of factors governing the sensor response of sol-gel derived sensor thin films. It can be concluded that the sensor response for gas phase and dissolved oxygen is optimised for more hydrophobic films. It was shown that the thickness stabilisation times for sol-gel thin films fabricated form organically modified precursors were much reduced compared to unmodified films and the hydrophobicity of the sensor films increased by introducing a hydrophobic group such as $-CH_3$ or $-C_2H_5$ into the sol-gel matrix. This hydrophobicity facilitated the sensor response in dissolved oxygen by increasing the partitioning effect of the oxygen out of solution. This was shown by the quenching response results in chapter 7. The increasing hydrophobicity of the films also improved gas phase sensor performance by reducing the effect of humidity on the response. From the range of films studied for this project, it can be concluded that the optimum films for both gas phase and DO sensing are those fabricated from ETES and ETMS.

8.2 Suggestions for Further work

This project looked at the effect of introducing a non-hydrolisable Si-C bond into the sol-gel matrix and investigated the properties of thin films fabricated for such precursors. The next stage in this investigation would be to expand the aliphatic group from ethyl to butyl and to investigate the effect that this has on film properties.

The fluorescence decay time apparatus used in this project was too inaccurate to determine the effect of the sol-gel matrix on the decay time of the entrapped dye complex. The next stage of this investigation would be to use a pulsed LED system as discussed in section 7.5.

8.3 Publications Arising From this Project

P. Lavin, C.M. McDonagh, B.D. MacCraith: **Optimisation of Ormosil Films for Optical Sensor Applications**, accepted for publication in *J. Sol-Gel Sci. Technol.* (1998)